

Independent origins of fetal liver haematopoietic stem and progenitor cells

<https://doi.org/10.1038/s41586-022-05203-0>

Received: 10 March 2021

Accepted: 5 August 2022

Published online: 14 September 2022

 Check for updates

Tomomasa Yokomizo^{1,2}✉, Takako Ideue¹, Saori Morino-Koga³, Cheng Yong Tham⁴, Tomohiko Sato⁵, Naoki Takeda⁶, Yoshiaki Kubota⁷, Mineo Kurokawa⁵, Norio Komatsu⁸, Minetaro Ogawa³, Kimi Araki^{6,9}, Motomi Osato^{1,4,10} & Toshio Suda^{1,4}✉

Self-renewal and differentiation are tightly controlled to maintain haematopoietic stem cell (HSC) homeostasis in the adult bone marrow^{1,2}. During fetal development, expansion of HSCs (self-renewal) and production of differentiated haematopoietic cells (differentiation) are both required to sustain the haematopoietic system for body growth^{3,4}. However, it remains unclear how these two seemingly opposing tasks are accomplished within the short embryonic period. Here we used *in vivo* genetic tracing in mice to analyse the formation of HSCs and progenitors from intra-arterial haematopoietic clusters, which contain HSC precursors and express the transcription factor hepatic leukaemia factor (HLF). Through kinetic study, we observed the simultaneous formation of HSCs and defined progenitors—previously regarded as descendants of HSCs⁵—from the HLF⁺ precursor population, followed by prompt formation of the hierarchical haematopoietic population structure in the fetal liver in an HSC-independent manner. The transcription factor EVI1 is heterogeneously expressed within the precursor population, with EVI1^{hi} cells being predominantly localized to intra-embryonic arteries and preferentially giving rise to HSCs. By genetically manipulating EVI1 expression, we were able to alter HSC and progenitor output from precursors *in vivo*. Using fate tracking, we also demonstrated that fetal HSCs are slowly used to produce short-term HSCs at late gestation. These data suggest that fetal HSCs minimally contribute to the generation of progenitors and functional blood cells before birth. Stem cell-independent pathways during development thus offer a rational strategy for the rapid and simultaneous growth of tissues and stem cell pools.

The standard hierarchical model of haematopoiesis places HSCs at the apex of the haematopoietic lineage, followed by various descendant progenitor cells that emerge in a stepwise manner². These varied intermediate progenitors were discovered in the bone marrow through sorting based on cell surface markers, *in vitro* colony-forming assays and transplantation experiments^{6–8}, with the hierarchical progression of HSCs to mature blood cells being subsequently described through genetic lineage tracing in adult mice^{9–12}. Similar to adult bone marrow, the HSC–progenitor hierarchy in the late gestational fetal liver is believed to be established through the differentiation of fetal HSCs^{5,13–15} (Extended Data Fig. 1). However, this notion assumes that the relationship between HSCs and progenitors is conserved from embryo to adult. Furthermore, considering the extremely rapid formation of the HSC–progenitor hierarchy in the mouse fetal liver¹⁵ (three to four days after HSC emergence), it is difficult to apply the kinetics observed in adult-stage tracing to that of fetal HSCs.

Identification of HLF⁺ pre-HSPCs

At embryonic day (E) 9.5–11.5 in the mouse, HSCs or progenitors are generated from endothelial cells through the process of endothelial-to-haematopoietic transition¹⁶ (EHT). Specifically, flattened haemogenic endothelia transform into rounded haematopoietic cells¹⁷ and then into cell aggregates called haematopoietic clusters¹⁸. These clusters are thought to contain HSC precursors^{19,20} (pre-HSCs) that colonize the fetal liver before or after they mature into fully functional HSCs^{21,22}. Here we analysed HSCs and lineage-restricted progenitor formation during embryonic development using an *in vivo* tracing strategy in Cre recombinase (Cre) tracer mice. To standardize the developmental stage of labelling, we generated a creERT2 strain using *Hlf*, which is expressed exclusively in KIT⁺ haematopoietic clusters and not in endothelial cells²³ (Extended Data Fig. 2a–g).

¹International Research Center for Medical Sciences, Kumamoto University, Kumamoto, Japan. ²Microscopic and Developmental Anatomy, Tokyo Women's Medical University, Tokyo, Japan.

³Department of Cell Differentiation, Institute of Molecular Embryology and Genetics, Kumamoto University, Kumamoto, Japan. ⁴Cancer Science Institute of Singapore, National University of Singapore, Singapore, Singapore. ⁵Department of Hematology and Oncology, Graduate School of Medicine, The University of Tokyo, Tokyo, Japan. ⁶Institute of Resource Development and Analysis, Kumamoto University, Kumamoto, Japan. ⁷Department of Anatomy, Keio University School of Medicine, Tokyo, Japan. ⁸Department of Hematology, Juntendo University Graduate School of Medicine, Tokyo, Japan. ⁹Center for Metabolic Regulation of Healthy Aging, Kumamoto University, Kumamoto, Japan. ¹⁰Department of Paediatrics, National University of Singapore, Singapore, Singapore. ✉e-mail: tomoyokomizo@gmail.com; csits@nus.edu.sg

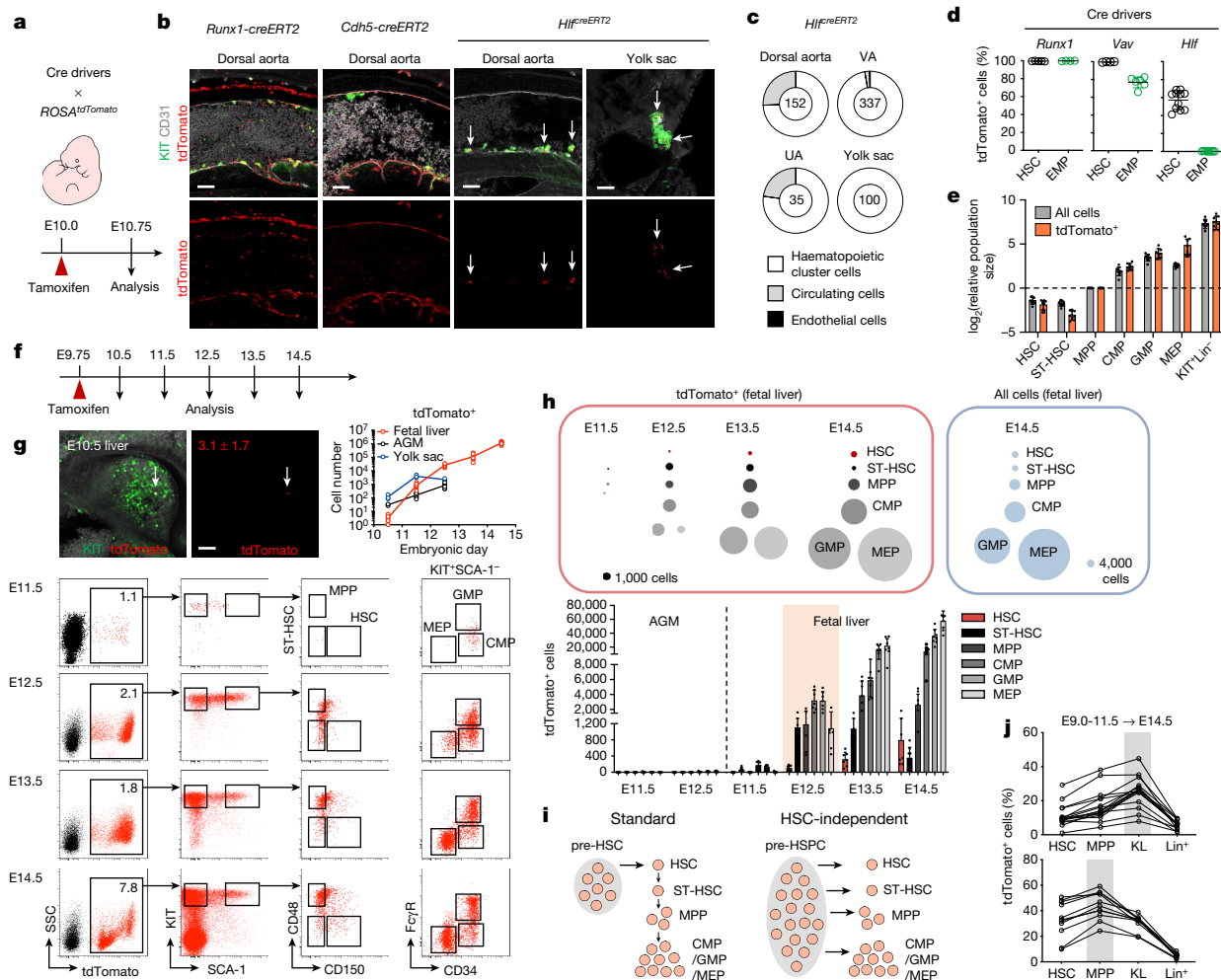


Fig. 1 | Fate tracing of HCCs reveals HSC-independent progenitor formation from pre-HSPCs. **a–c.** Specific labelling of HCCs in *Hif^{creERT2}* mice. **a.** Schematic of cell labelling by Cre driver lines. **b.** Whole-mount immunostaining analysis of labelled cells in *Runx1-creERT2::ROSA26tdTomato* (36 somite pairs (sp)), *Cdh5-creERT2::ROSA26tdTomato* (36 sp) and *Hif^{creERT2}ROSA26tdTomato* (37 sp) embryos. White arrows indicate *tdTomato*⁺ cells. Scale bars, 50 μ m. *Cdh5* is also known as *VEcad*. **c.** Frequency of HCCs, circulating KIT⁺ cells and endothelial cells among *Hif^{creERT2}*-labelled cells. Numbers in the centre of the doughnut chart indicate the total number of *tdTomato*⁺ cells analysed. Combined data are from 6 embryos (35–39 sp). VA, vitelline artery; UA, umbilical artery. **d.** Frequency of *tdTomato*⁺ cells in HSC and EMP fractions from *Runx1-creERT2::ROSA26tdTomato* (HSC, $n = 5$; EMP, $n = 4$), *Vav-cre::ROSA26tdTomato* (HSC, $n = 4$; EMP, $n = 6$) and *Hif^{creERT2}ROSA26tdTomato* (HSC, $n = 11$; EMP, $n = 8$) embryos. **e.** Relative population size among all cells and *Hif^{creERT2}ROSA26tdTomato* embryos were administered with tamoxifen at E9.75 and were analysed at E14.5 ($n = 8$).

f–h. Kinetic analysis of HSC and progenitor formation from *Hif^{creERT2}*-labelled cells. **f.** Schematic of tamoxifen treatment and analysis. **g.** Top left, fetal liver at E10.5 (35 sp). The average number of *tdTomato*⁺ cells (arrow) is shown. Scale bar, 50 μ m. Top right, the number of *tdTomato*⁺ cells in fetal liver, AGM and yolk sac. Bottom, representative flow cytometry plots of *Hif^{creERT2}*-labelled cells in the fetal liver (red dots). **h.** Formation of hierarchical haematopoietic structure from HLF⁺ cells in the fetal liver. Top, circle size represents the population size of defined fractions among *Hif^{creERT2}*-labelled cells and all cells. Bottom, quantification of *tdTomato*⁺ cells. The numbers of analysed embryos are summarized in the Source Data. **i.** Hierarchical haematopoietic structure formation in the fetal liver. Left, the standard model. Right, a HSC-independent model. **j.** HSC-independent formation of progenitors. KL-dominant (top; 16 embryos) and MPP-dominant (bottom; 11 embryos) types were extracted from a total of 56 embryos (tamoxifen at E9.0–11.5), as shown in Extended Data Fig. 3d. Data are mean \pm s.d.

Tamoxifen was first administered to *Hif^{creERT2}ROSA26tdTomato* embryos at E10.0, with embryos collected after 18 h (E10.75) (Fig. 1a). The localization of labelled cells was determined using whole-mount immunostaining analysis. As expected, labelled cells were detected within KIT⁺ haematoopoietic clusters localized to the dorsal aorta ($5.8\% \pm 2.8\%$, mean \pm sd), vitelline artery ($18\% \pm 7.9\%$), umbilical artery ($5.5\% \pm 1.8\%$) and yolk sac ($6.2\% \pm 0.39\%$) (Fig. 1b and Extended Data Fig. 2h,i); by contrast, *tdTomato*⁺ endothelial cells were rarely observed (1 out of 624 *tdTomato*⁺ cells; Fig. 1c). Erythro-myeloid progenitors²⁴ (EMPs) were not marked in *Hif^{creERT2}* mice (Fig. 1d and Extended Data Fig. 2j–m), consistent with our previous characterization of *Hif^{tdTomato}* reporter mice²³. This absence of marking avoids potential contamination of EMP or EMP progenies in our tracing analyses. We then collected embryos at E14.5 and analysed cells in the fetal liver. Cre-labelled cells were observed in

CD150⁺CD48⁺KIT⁺SCA-1⁺Lineage(Lin)[–] (*CD150⁺CD48⁺KSL*) HSCs²⁵ and other defined progenitor fractions, such as *CD150[–]CD48⁺KSL* multipotent progenitors (MPPs) and *CD34⁺FcyR[–]KIT⁺Lin[–]* (*CD34⁺FcyR[–]KL*) common myeloid progenitors (CMPs). We measured similar relative population sizes to that of the total cell count (Fig. 1e), indicating that *Hif^{creERT2}* tracing covers most of the HSC and progenitor lineages in the fetal liver at E14.5. Thus, *Hif^{creERT2}ROSA26tdTomato* tracing recapitulates haematopoietic hierarchy formation in fetal liver.

We next performed a time-course analysis of HSC and progenitor formation from HLF⁺ precursors (tamoxifen at E9.75; Fig. 1f). At E10.5, we observed few (3.1 ± 1.7 , $n = 7$) *tdTomato*⁺KIT⁺ cells in the fetal liver (Fig. 1g), suggesting that most of the labelled cells in the aorta–gonad–mesonephros (AGM) and yolk sac do not migrate to the fetal liver at this stage. At E11.5, we measured 869 ± 401 *tdTomato*⁺ cells in the fetal

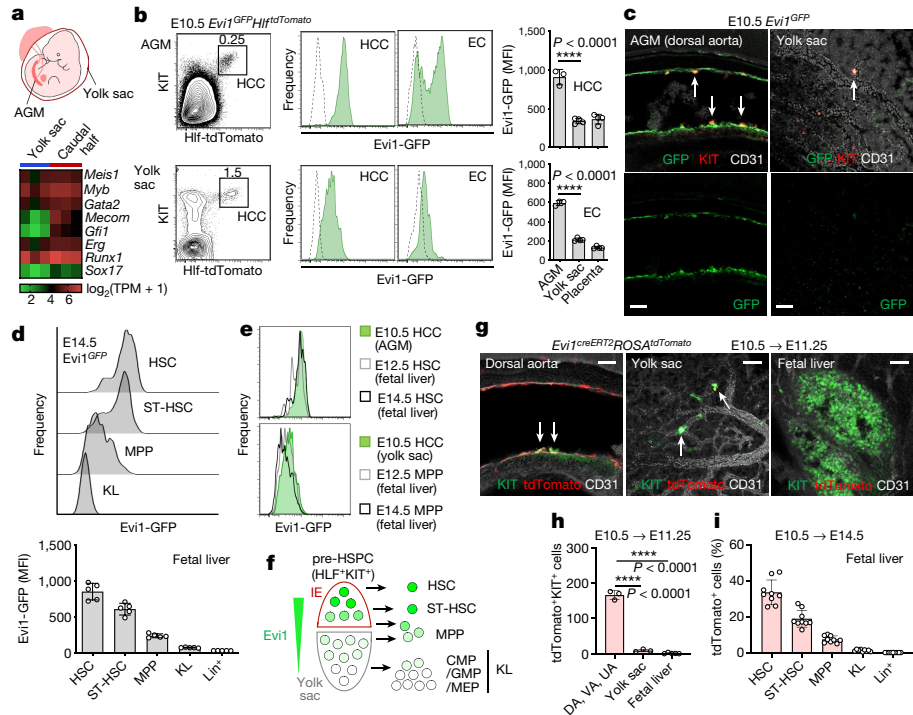


Fig. 2 | Intra-embryonic EVI1^{hi} cells preferentially generate HSCs.

a, Transcriptome analysis of transcription factors in HLF⁺KIT⁺CD45⁻ HCCs isolated from the caudal half of the embryo including the AGM or yolk sac at E10.5 (33–35 sp). TPM, transcripts per million base pairs. Mecom includes the *Evi1* locus. **b**, Flow cytometry analysis of Evi1-GFP expression in E10.5 (32–36 sp) *Evi1*^{GFP/+}*Hif*^{tdTomato/+} embryos. Representative flow cytometry (left) and frequency (middle) plots of *Evi1*^{GFP/+}*Hif*^{tdTomato/+} (green) and *Evi1*^{+/+}*Hif*^{tdTomato/+} (black dashed) embryos. Right, mean fluorescence intensity (MFI) of Evi1-GFP in HCC and endothelial cell (EC) fractions (AGM, $n = 3$; yolk sac, $n = 4$; placenta, $n = 4$). **c**, Whole-mount immunostaining analysis of E10.5 (33 sp) *Evi1*^{GFP} embryos. Arrows indicate KIT⁺ haematopoietic clusters. Scale bars, 50 μ m. **d**, Evi1-GFP expression in E14.5 fetal livers. Top, representative flow cytometry plot.

Bottom, MFI of Evi1-GFP in haematopoietic lineages ($n = 5$). **e**, Comparison of Evi1-GFP expression among E10.5, E12.5 and E14.5 embryos. **f**, Model of hierarchical haematopoietic structure formation from pre-HSPCs. EVI1 expression level determines the fate of pre-HSPCs. IE, intra-embryonic region; HSPC, haematopoietic stem and progenitor cells. **g–i**, Lineage tracing of EVI1^{hi} cells. *Evi1*^{creERT2}*ROSA*^{tdTomato} embryos were administered with tamoxifen at E10.5 and were analysed at E11.25 (**g, h**; dorsal aorta (DA), vitelline artery and umbilical artery, $n = 3$; yolk sac, $n = 3$; fetal liver, $n = 4$) and E14.5 (**i**; $n = 9$). **g**, Whole-mount immunostaining analysis; arrows indicate KIT⁺ haematopoietic clusters. Scale bars, 50 μ m. Data are mean \pm s.d. **b, h**, One-way ANOVA with Tukey–Kramer test.

liver (Fig. 1g,h), with phenotypes that were reminiscent of haematopoietic cluster cells (HCCs), displaying homogeneous expression of KIT and CD34, and low or no SCA-1 expression (Fig. 1g and Extended Data Fig. 3a,b). Thus, the labelled cells still retained the characteristics of nascent haematopoietic cells generated from endothelium in the dorsal aorta or yolk sac. One day later (E12.5), the tdTomato⁺SCA-1⁺KIT⁺ fraction appeared, as did phenotypically defined HSCs and other progenitors, including MPPs, granulocyte macrophage progenitors (GMPs), and megakaryocyte erythrocyte progenitors (MEPs) (Fig. 1g,h and Extended Data Fig. 3c). These kinetic data strongly suggest that HSCs and progenitors are generated independently from HLF⁺KIT⁺ pre-haematopoietic stem and progenitor cell (pre-HSPC) population almost simultaneously and form a hierarchical-like structure in the fetal liver (Fig. 1i).

Finally, we analysed the fate of HCCs at different stages by varying the stage of tamoxifen delivery (E9.0–11.5). When delivered at earlier stages (E9.0–10.25), we observed a higher labelling frequency in the progenitors than in the HSCs (Fig. 1h and Extended Data Fig. 3d), which could be categorized into two types: KL-dominant and MPP-dominant (Fig. 1j). The existence of the KL-dominant type suggests that KL generation occurs independently of HSCs and MPPs.

EVI1^{hi} cells in intra-embryonic regions

The parallel emergence of HSCs and various progenitors from HLF⁺KIT⁺ precursors implied a heterogeneity within the pre-HSPC population. To understand transcriptional diversity within these pre-HSPCs, we

performed single-cell RNA-seq analysis of the dorsal aorta and its surrounding tissues, including the fetal liver (Extended Data Fig. 4a). We identified a developmental trajectory from endothelial to haematopoietic populations and an intermediate HLF^{hi}KIT^{hi} fraction (Extended Data Fig. 4b–d). Within this putative pre-HSPC population, there was a heterogeneous expression of stem-associated genes (*Mecom*, *Gfi1* and *Procr*) and committed haematopoietic marker genes (*Cd48*, *Flt3*, *Il7r* and *Csf1r*) (Extended Data Fig. 4e–g), suggesting that stem and progenitor cell fates are segregated at an early stage. This was confirmed by analysing published datasets (Extended Data Fig. 4h–m). Because most HSCs are believed to be generated from the intra-embryonic region^{26,27}, we hypothesized that a stem cell-specifying factor might be predominantly expressed by pre-HSPCs localized in the embryo proper. Using bulk RNA-seq analysis, we compared the expression of transcription factor genes in HLF⁺KIT⁺CD45⁻ nascent HCCs²³ between the caudal half region and the yolk sac. We found a high expression of *Mecom* (also known as *Mds1* and *Evi1* complex locus) in the caudal half region (Fig. 2a). The scRNA-seq data (Extended Data Fig. 4e) also identified *Mecom* expression at the endothelial stage, which was maintained in the HLF^{hi} pre-HSPC fraction. We therefore focused further detailed analysis on *Evi1*.

EVI1 is a critical regulator of adult HSCs and is required for the formation of fetal HSCs^{23,28,29}. Using *Evi1*^{GFP} reporter mice, in which EVI1 and GFP are expressed under control of the endogenous *Evi1* regulatory element, we analysed EVI1 expression in the AGM, yolk sac and placenta at E10.5. Consistent with RNA-seq data, EVI1 was highly expressed in

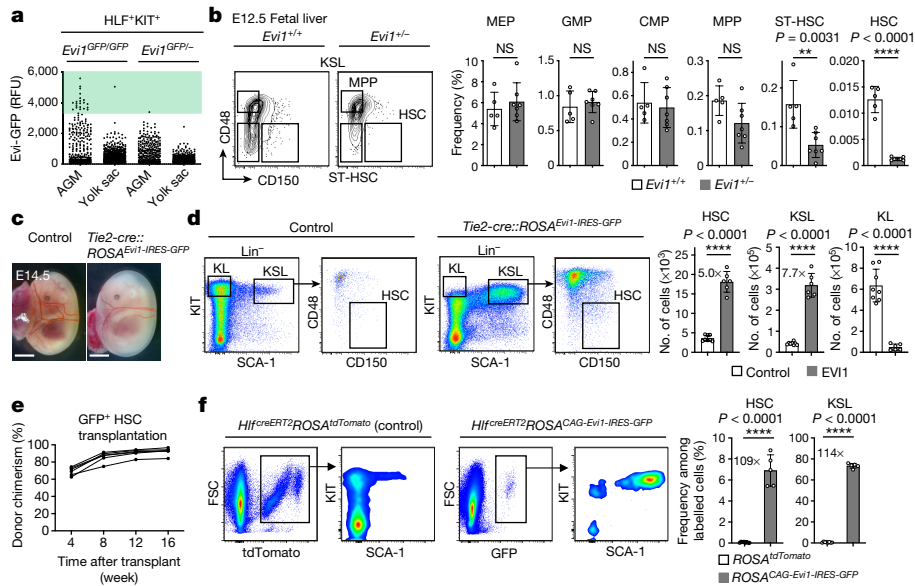


Fig. 3 | EVI1 expression level determines the fate of pre-HSPCs. **a**, Hemizygous dosage effect of *Evi1*. EVI1 expression in HLF⁺KIT⁺ pre-HSPCs at E11.5. Fluorescence of Evi1-GFP was quantified from 3 independent flow cytometry analyses and is expressed in relative fluorescence units (RFU) ($n = 400$ cells from 4 *Evi1^{GFP/GFP}* *Hif^{tdTomato/+}* AGM; $n = 1,320$ cells from 4 *Evi1^{GFP/GFP}* *Hif^{tdTomato/+}* AGM; $n = 875$ cells from 3 *Evi1^{GFP/+}* *Hif^{tdTomato/+}* yolk sac). Note that GFP^{hi} cells (green-shaded area) are absent from *Evi1*-GFP-heterozygous embryos. **b**, Specific decrease in the stem cell fraction in *Evi1*-heterozygous embryos at E12.5. Left, representative flow cytometry plots. Right, frequency of HSC and progenitor fractions (*Evi1^{+/+}* mice, $n = 5$; *Evi1⁺⁻* mice, $n = 7$). **c**, Ectopic expression of EVI1 in endothelial cells. *Tie2-cre::ROSA^{Evi1-IRES-GFP}* embryos show mild anaemia. Scale

bars, 300 μ m. **d**, Forced expression of EVI1 in endothelial cells changes the fate of pre-HSPCs. Left, representative flow cytometry plot of E14.5 fetal liver cells. Right, number of HSCs and progenitor cells (control, *Tie2-cre* and *ROSA^{Evi1-IRES-GFP}* embryos, $n = 8$; *Tie2-cre::ROSA^{Evi1-IRES-GFP}* embryos, $n = 6$). **e**, Transplantation experiments. Irradiated mice were transplanted with 100 GFP^{hi} HSCs isolated from E14.5 *Tie2-cre::ROSA^{Evi1-IRES-GFP}* fetal liver ($n = 6$). **f**, Fate tracing of EVI1-induced HLF⁺ cells. *Hif^{creERT2}ROSA^{tdTomato}* embryos (control) and *Hif^{creERT2}ROSA^{CAG-Evi1-IRES-GFP}* embryos were administered with tamoxifen at E9.75 and were analysed at E14.5. Left, representative flow cytometry plots of E14.5 fetal liver cells. Right, frequency of HSCs and KSL cells among labelled cells (*Hif^{creERT2}ROSA^{tdTomato}* embryos, $n = 8$; *Hif^{creERT2}ROSA^{CAG-Evi1-IRES-GFP}* embryos, $n = 5$). Data are mean \pm s.d. **b,d,f**, Two-sided unpaired Student's *t*-test. NS, not significant.

HCCs (HLF⁺KIT⁺) and in the endothelial cell fraction (CD31⁺CD45⁻CD41⁺) within the AGM region (Fig. 2b). This was confirmed in the whole-mount immunostaining analysis, with strong Evi1-GFP expression in the endothelial layer of the dorsal aorta, vitelline and umbilical arteries, and low expression in the yolk sac arteries (Fig. 2c and Extended Data Fig. 5); GFP^{lo} cells were restricted to the artery around the entrance of the yolk sac (Extended Data Fig. 5a).

EVI1^{hi} cells preferentially generate HSCs

High EVI1 expression has been reported in HSCs in the adult bone marrow, with lower levels being measured in progenitors and mature cells in a hierarchical manner³⁰. We noted a similar expression pattern in the fetal liver at E14.5 (Fig. 2d), as well as a similar fluorescence intensity of Evi1-GFP in E14.5 and Evi1-GFP E12.5 HSCs as in E10.5 HCCs (HLF⁺KIT⁺) (Fig. 2e). Moreover, Evi1-GFP expression in E14.5 and E12.5 MPPs was similar to that in E10.5 yolk sac cluster cells (Fig. 2e). Given that HSCs and progenitors in the fetal liver are produced separately from precursors (Fig. 1i), we speculated that EVI1^{hi} cells within pre-HSPCs (HLF⁺KIT⁺ cells) preferentially give rise to HSCs, with EVI1^{lo} or EVI1⁻ cells becoming progenitors (Fig. 2f). To test this hypothesis, we generated *Evi1^{creERT2}* knock-in mice to trace the fate of EVI1^{hi} cells in vivo (Extended Data Fig. 6a-d and Supplementary Information). We administered tamoxifen to *Evi1^{creERT2}ROSA^{tdTomato}* mice at E10.5 and analysed embryos after 18 h (E11.25) by whole-mount immunostaining. Consistent with analysis of *Evi1^{GFP}* embryos, tdTomato⁺KIT⁺ cells were detected almost exclusively in the major arteries within the embryo proper (Fig. 2g,h and Extended Data Fig. 6e,f). We then analysed the fate of the marked cells in fetal livers at E14.5. As predicted, the labelling frequency was highest in the HSC fraction (38.2% \pm 7.4%), with a significantly lower level of

label detected in MPP (9.3% \pm 2.3%) and KL (1.4% \pm 0.64%) populations (Fig. 2i and Extended Data Fig. 6g,h). In addition, dual-colour tracing with the *ROSA^{tdTomato/YFP}* reporter showed the EVI1 expression level to be correlated with lineage output from precursors (Extended Data Fig. 7a-c). Together, these data indicate that intra-embryonic EVI1^{hi} cells preferentially generate HSCs and that the gradient of EVI1 expression regulates the fate of pre-HSPCs (Fig. 2f, Extended Data Fig. 7d-g and Supplementary Information).

EVI1 level determines the fate of pre-HSPCs

To validate the importance of EVI1 expression in pre-HSPC fate determination, we attempted to deplete EVI1^{hi} cells from the pre-HSPC fraction. We examined the expression of EVI1 in individual pre-HSPCs (HLF⁺KIT⁺ cells) using a the *Evi1^{GFP}* knock-in reporter³⁰. In *Evi1-GFP* homozygous embryos (*Evi1^{GFP/GFP}*), Evi1-GFP^{hi} cells were detected exclusively in the AGM, whereas *Evi1-GFP* heterozygous embryos (*Evi1^{GFP/+}*; in which a single *Evi1-IRES-GFP* allele is deleted) lacked Evi1-GFP^{hi} cells (Fig. 3a). Thus, depletion of EVI1^{hi} cells could be achieved using *Evi1*-heterozygous (*Evi1^{+/+}*) embryos. We therefore next analysed HSC and progenitor fractions in *Evi1^{+/+}* fetal livers at E12.5. As predicted by our model (Fig. 2f), we observed a specific decrease in the HSC fraction (9.9-fold decrease) in *Evi1^{+/+}* embryos, indicating that HSC formation is most sensitive to EVI1 expression levels (Fig. 3b and Extended Data Fig. 8a). Despite the massive reduction in HSC production, counts of other progenitor populations (CMPs, GMPs and MEPs) were maintained (Fig. 3b and Extended Data Fig. 8b-d). These findings strongly support the notion that most progenitors in the fetal liver are generated independently of HSCs.

We next tested whether the ectopic EVI1 expression alters precursor fate in vivo. We generated *ROSA26^{Evi1-IRES-GFP}* mice (Extended Data Fig. 9a)

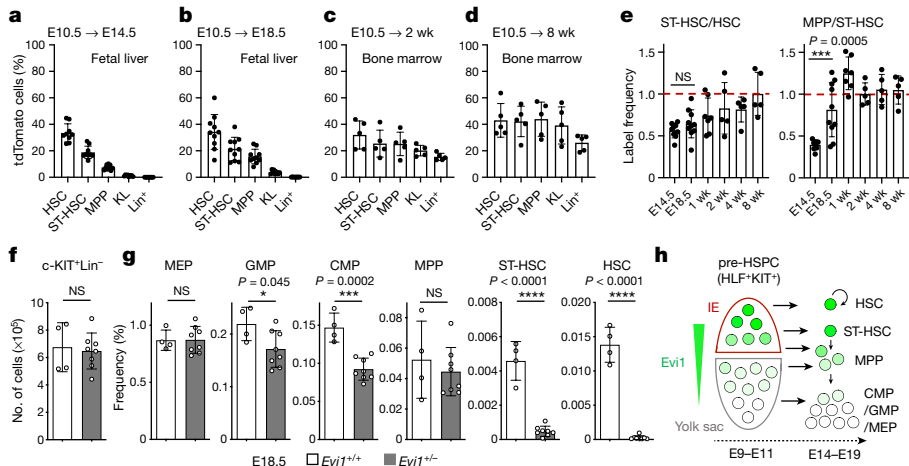


Fig. 4 | Fetal HSCs minimally contribute to progenitors and mature cells.

a–d, Lineage tracing of *Evi1^{creERT2}ROSA^{tdTomato}* embryos were administered with tamoxifen at E10.5 and were analysed at E14.5 (**a**; $n = 9$), E18.5 (**b**; $n = 10$), 2 weeks (**wk**) (**c**; $n = 5$) and 8 weeks (**d**; $n = 5$). **e**, Fetal HSCs minimally contribute to ST-HSCs. Labelled progression from HSCs to ST-HSCs (left) and ST-HSCs to MPPs (right). $n = 9$ (E14.5), $n = 10$ (E18.5), $n = 7$ (1 week), $n = 5$ (2 weeks),

$n = 5$ (4 weeks) and $n = 5$ (8 weeks) mice. **f,g**, Minimal influence of HSC deficiency on embryonic haematopoiesis (*Evi1^{+/+}* mice, $n = 4$; *Evi1^{-/-}* mice, $n = 8$). **f**, Total number of KIT⁺Lin⁻ cells in E18.5 fetal livers. **g**, Frequency of HSPC fractions in E18.5 fetal liver. **h**, Model of HSC-independent formation and maintenance of the embryonic haematopoietic system. Data are mean \pm s.d. One-way ANOVA with Dunnett's test (**e**) and two-sided unpaired Student's *t*-test (**f,g**).

to induce EVI1 expression in a Cre-dependent manner. This mouse was then crossed with the *Cdh5-creERT2* or *Tie2-cre* line to induce EVI1 in endothelial cells. In *Cdh5-creERT2::ROSA26^{Evi1-IRES-GFP}* embryos (tamoxifen at E9.5), we measured an approximately twofold increase in the population of KSL cell and HSC fractions, indicating that HSCs can be induced by the ectopic expression of EVI1 (Extended Data Fig. 9b–d). Of note, in *Tie2-cre::ROSA^{Evi1-IRES-GFP}* embryos, there was a significant increase in the numbers of HSC (5.0-fold) and KSL (7.7-fold) cells in the fetal liver (Fig. 3c–e and Extended Data Fig. 9e–h), and a near absence of the KL fraction (Fig. 3d). These results suggest that KL precursors can be redirected into immature KSL precursors by EVI1.

To determine whether a fate change occurs within endothelial cells (before EHT) or in the HLF⁺ pre-HSPC fraction (after EHT), we next crossed *ROSA^{Evi1-IRES-GFP}* mice with the *Hlf^{creERT2}* line. However, the recombination rate was too low to analyse the effect of EVI1 expression in HLF⁺ cells. We therefore generated a novel *ROSA26^{CAG-Evi1-IRES-GFP}* (high recombination type) mouse line to obtain a sufficient number of recombined cells (Extended Data Fig. 9i,j). Since this *ROSA26^{CAG-Evi1-IRES-GFP}* mouse also functions as a tracing system (because of the inserted GFP gene), we can analyse the fate of EVI1-induced HLF⁺ cells. Under normal conditions (*Hlf^{creERT2}ROSA^{tdTomato}*), most of the labelled HLF⁺ cells gave rise to KIT⁺SCA-1⁺ or KIT⁺SCA-1⁻ cells (Fig. 3f). Notably, when EVI1 was induced, $73.5\% \pm 2.2\%$ of the induced cells (that is, GFP⁺ cells) gave rise to KIT⁺SCA-1⁺ cells, including the HSC fraction (Fig. 3f). These results confirm that fate determination relies on the expression level of EVI1 in pre-HSPCs.

Tracing of HSC output during development

HSCs are reported to rapidly expand in the fetal liver^{31–33}. However, their contribution to descendant progenitors during late gestation remains unclear. Since *Evi1^{creERT2}* tracing preferentially marks HSCs at E14.5 (Fig. 2i), we next examined the progression of labelling from HSCs to progenitors after E14.5 (Fig. 4a–d). If labelled HSCs differentiate to short-term HSCs (ST-HSCs), the ST-HSC/HSC ratio would increase and finally reach unity (full equilibration of label). We found that although the frequency of the labelled MPP fraction increased between E14.5 and E18.5, that of the labelled ST-HSC remained constant (Fig. 4e). This suggests that there is no or little influx of HSCs into ST-HSCs; if this were so, the absolute number of ST-HSCs would have decreased after E14.5. To confirm this, we compared the number of HSCs and progenitors in

the fetal liver between E14.5 and E18.5. Indeed, only ST-HSC numbers decreased after E14.5 (Extended Data Fig. 10a), indicating that HSCs contribute minimally to the production of descendant progenitors during the embryonic stage. Consistent with this idea, *Evi1^{-/-}* embryos, which exhibit defective HSC formation (Fig. 3b and Extended Data Fig. 8c), retained almost normal numbers of KIT⁺ progenitors at E18.5 (Fig. 4f,g and Extended Data Fig. 10b), suggesting that the embryonic haematopoietic system can be maintained with minimal involvement of HSCs.

Discussion

Here we demonstrate that haematopoietic progenitors in E14.5 fetal livers are generated independently of HSCs. HSCs and various intermediate progenitors derived from different precursors from different locations converge in the fetal liver to form its hierarchical structure in situ. It is thus plausible that a blueprint of the tree-like hierarchical structure is embedded in the precursor state. Our finding is largely in line with a recent in vitro functional study demonstrating that the emergence of multipotential progenitors from the haemogenic endothelium is uncoupled from the emergence of HSCs³⁴. We did not observe any HSC contribution to the formation of descendant progenitors during late gestation and suggest that most of the blood cells in the embryo are formed in a HSC-independent manner (Fig. 4h). This system could reasonably expand the stem cell pool and supply differentiated cells within a short period of time; such a concept may be common to regenerative situations and haematopoietic system formation in vertebrates^{35,36}.

We further highlight that the EVI1 expression level is important for specifying HSCs within pre-HSPC populations in vivo. This feature would also apply to the in vitro induction of HSCs from pluripotent cells. Whereas several research groups have sought to activate stem cell programmes by the combinatorial expression of several (two to seven) transcription factors^{37–40}, we suggest that the transient induction of a single factor at the appropriate precursor stage (pre-HSPC stage) might be able to amplify the physiological developmental pathway of HSCs in vitro.

Online content

Any methods, additional references, Nature Research reporting summaries, source data, extended data, supplementary information, acknowledgements, peer review information; details of author contributions

and competing interests; and statements of data and code availability are available at <https://doi.org/10.1038/s41586-022-05203-0>.

1. Haas, S., Trumpp, A. & Milson, M. D. Causes and consequences of hematopoietic stem cell heterogeneity. *Cell Stem Cell* **22**, 627–638 (2018).
2. Laurenti, E. & Gottgens, B. From haematopoietic stem cells to complex differentiation landscapes. *Nature* **553**, 418–426 (2018).
3. Dzierzak, E. & Bigas, A. Blood development: hematopoietic stem cell dependence and independence. *Cell Stem Cell* **22**, 639–651 (2018).
4. Ivanovs, A. et al. Human haematopoietic stem cell development: from the embryo to the dish. *Development* **144**, 2323–2337 (2017).
5. Traver, D. et al. Fetal liver myelopoiesis occurs through distinct, prospectively isolatable progenitor subsets. *Blood* **98**, 627–635 (2001).
6. Adolfsson, J. et al. Identification of Flt3⁺ lympho-myeloid stem cells lacking erythro-megakaryocytic potential a revised road map for adult blood lineage commitment. *Cell* **121**, 295–306 (2005).
7. Akashi, K., Traver, D., Miyamoto, T. & Weissman, I. L. A clonogenic common myeloid progenitor that gives rise to all myeloid lineages. *Nature* **404**, 193–197 (2000).
8. Yamamoto, R. et al. Clonal analysis unveils self-renewing lineage-restricted progenitors generated directly from hematopoietic stem cells. *Cell* **154**, 1112–1126 (2013).
9. Busch, K. et al. Fundamental properties of unperturbed haematopoiesis from stem cells in vivo. *Nature* **518**, 542–546 (2015).
10. Chapple, R. H. et al. Lineage tracing of murine adult hematopoietic stem cells reveals active contribution to steady-state hematopoiesis. *Blood Adv.* **2**, 1220–1228 (2018).
11. Sawai, C. M. et al. Hematopoietic stem cells are the major source of multilineage hematopoiesis in adult animals. *Immunity* **45**, 597–609 (2016).
12. Sawen, P. et al. Murine HSCs contribute actively to native hematopoiesis but with reduced differentiation capacity upon aging. *eLife* **7**, e41258 (2018).
13. Draper, J. E. et al. A novel prospective isolation of murine fetal liver progenitors to study in utero hematopoietic defects. *PLoS Genet.* **14**, e1007127 (2018).
14. Notta, F. et al. Distinct routes of lineage development reshape the human blood hierarchy across ontogeny. *Science* **351**, aab2116 (2016).
15. Orkin, S. H. & Zon, L. I. Hematopoiesis: an evolving paradigm for stem cell biology. *Cell* **132**, 631–644 (2008).
16. Chen, M. J., Yokomizo, T., Zeigler, B. M., Dzierzak, E. & Speck, N. A. Runx1 is required for the endothelial to haematopoietic cell transition but not thereafter. *Nature* **457**, 887–891 (2009).
17. Boisset, J. C. et al. In vivo imaging of haematopoietic cells emerging from the mouse aortic endothelium. *Nature* **464**, 116–120 (2010).
18. Yokomizo, T. & Dzierzak, E. Three-dimensional cartography of hematopoietic clusters in the vasculature of whole mouse embryos. *Development* **137**, 3651–3661 (2010).
19. Taoudi, S. et al. Extensive hematopoietic stem cell generation in the AGM region via maturation of VE-cadherin⁺CD45⁺ pre-definitive HSCs. *Cell Stem Cell* **3**, 99–108 (2008).
20. Zhou, F. et al. Tracing haematopoietic stem cell formation at single-cell resolution. *Nature* **533**, 487–492 (2016).
21. Kieusseian, A., Brunet de la Grange, P., Burlen-Defranoux, O., Godin, I. & Cumano, A. Immature hematopoietic stem cells undergo maturation in the fetal liver. *Development* **139**, 3521–3530 (2012).
22. Rybtsov, S., Ivanovs, A., Zhao, S. & Medvinsky, A. Concealed expansion of immature precursors underpins acute burst of adult HSC activity in foetal liver. *Development* **143**, 1284–1289 (2016).
23. Yokomizo, T. et al. Hlf marks the developmental pathway for hematopoietic stem cells but not for erythro-myeloid progenitors. *J. Exp. Med.* **216**, 1599–1614 (2019).
24. McGrath, K. E. et al. Distinct sources of hematopoietic progenitors emerge before HSCs and provide functional blood cells in the mammalian embryo. *Cell Rep.* **11**, 1892–1904 (2015).
25. Kim, I., He, S., Yilmaz, O. H., Kiel, M. J. & Morrison, S. J. Enhanced purification of fetal liver hematopoietic stem cells using SLAM family receptors. *Blood* **108**, 737–744 (2006).
26. Medvinsky, A. & Dzierzak, E. Definitive hematopoiesis is autonomously initiated by the AGM region. *Cell* **86**, 897–906 (1996).
27. Cumano, A., Dieterlen-Lievre, F. & Godin, I. Lymphoid potential, probed before circulation in mouse, is restricted to caudal intraembryonic splanchnopleura. *Cell* **86**, 907–916 (1996).
28. Goyama, S. et al. Evi-1 is a critical regulator for hematopoietic stem cells and transformed leukemic cells. *Cell Stem Cell* **3**, 207–220 (2008).
29. Glass, C., Wilson, M., Gonzalez, R., Zhang, Y. & Perkins, A. S. The role of EVI1 in myeloid malignancies. *Blood Cells Mol. Dis.* **53**, 67–76 (2014).
30. Kataoka, K. et al. Evi1 is essential for hematopoietic stem cell self-renewal, and its expression marks hematopoietic cells with long-term multilineage repopulating activity. *J. Exp. Med.* **208**, 2403–2416 (2011).
31. Ema, H. & Nakuchi, H. Expansion of hematopoietic stem cells in the developing liver of a mouse embryo. *Blood* **95**, 2284–2288 (2000).
32. Gekas, C., Dieterlen-Liebre, F., Orkin, S. H. & Mikkola, H. K. The placenta is a niche for hematopoietic stem cells. *Dev. Cell* **8**, 365–375 (2005).
33. Khan, J. A. et al. Fetal liver hematopoietic stem cell niches associate with portal vessels. *Science* **351**, 176–180 (2016).
34. Dignam, T. et al. Multipotent progenitors and hematopoietic stem cells arise independently from hemogenic endothelium in the mouse embryo. *Cell Rep.* **36**, 109675 (2021).
35. Ema, H., Uchinomiya, K., Morita, Y., Suda, T. & Iwasa, Y. Repopulation dynamics of single haematopoietic stem cells in mouse transplantation experiments: Importance of stem cell composition in competitor cells. *J. Theor. Biol.* **394**, 57–67 (2016).
36. Ulloa, B. A. et al. Definitive hematopoietic stem cells minimally contribute to embryonic hematopoiesis. *Cell Rep.* **36**, 109703 (2021).
37. Doulatov, S. et al. Induction of multipotential hematopoietic progenitors from human pluripotent stem cells via respecification of lineage-restricted precursors. *Cell Stem Cell* **13**, 459–470 (2013).
38. Elcheva, I. et al. Direct induction of haematoendothelial programs in human pluripotent stem cells by transcriptional regulators. *Nat. Commun.* **5**, 4372 (2014).
39. Sugimura, R. et al. Haematopoietic stem and progenitor cells from human pluripotent stem cells. *Nature* **545**, 432–438 (2017).
40. Tsukada, M. et al. In vivo generation of engraftable murine hematopoietic stem cells by Gf1b, c-Fos, and Gata2 overexpression within Teratoma. *Stem Cell Reports* **9**, 1024–1033 (2017).

Publisher's note Springer Nature remains neutral with regard to jurisdictional claims in published maps and institutional affiliations.

Springer Nature or its licensor holds exclusive rights to this article under a publishing agreement with the author(s) or other rightsholder(s); author self-archiving of the accepted manuscript version of this article is solely governed by the terms of such publishing agreement and applicable law.

© The Author(s), under exclusive licence to Springer Nature Limited 2022

Methods

Mice and embryos

All mice were on the C57BL/6 background. *Hif*^{tdTomato}, *Runx1-creERT2* (*eR1-creERT2*), *Cdh5-creERT2*, *ROSA*^{tdTomato}, *ROSA*^{YFP}, *Vav-icre*, *Tie2-cre*, *Evi1*^{+/−}, *Evi1*^{GFP/+} mice have described previously^{23,28,30,41–46}. C57BL/6J mice and pregnant ICR mice (used as foster mothers) were purchased from Japan SLC. C57BL/6-Ly5.1(Ly5.1) mice were purchased from Sankyo-Lab Service. Embryos were generated by timed matings and were staged according to embryonic day, somite pairs (sp) and Theiler criteria (<http://www.emouseatlas.org/emap/home.html>). For adult bone marrow analysis, 8- to 12-week-old mice were used. All mice were bred in a specific pathogen-free animal facility (12 h light and 12 h dark) at Kumamoto University. All animal experiments were performed in accordance with institutional guidelines and were approved by the Animal Care and Use Committee of Kumamoto University.

Tamoxifen administration for Cre activation

Tamoxifen (T5648, Sigma) was dissolved in corn oil (Sigma-Aldrich) and was administered by oral gavage in the following amounts: *Hif*^{creERT2}*ROSA*^{tdTomato} (2.5 mg), *Runx1-creERT2::ROSA*^{tdTomato} (1.0 mg), *Cdh5-creERT2::ROSA*^{tdTomato} (0.5 mg), *Evi1*^{creERT2}*ROSA*^{tdTomato} (2.0 mg), *Evi1*^{GFP/creERT2}*ROSA*^{tdTomato} (4.0 mg), *Evi1*^{creERT2}*ROSA*^{tdTomato/YFP} (2.0 mg), *Cdh5-creERT2::ROSA*^{Evi1-IRES-GFP} (2.0 mg), *Hif*^{creERT2}*ROSA*^{Evi1-IRES-GFP} (2.5 mg), *Hif*^{creERT2}*ROSA*^{CAG-Evi1-IRES-GFP} (2.5 mg). Tamoxifen-administered pregnant mice were delivered by caesarean section at E19.5, and newborns were raised by ICR foster mothers.

Generation of the *Hif*^{creERT2} knock-in mouse

Hif^{creERT2} mice were generated by the insertion of a *T2A-creERT2* gene fusion before the endogenous stop codon within exon 4. The targeting vector was generated by modifying the *Hif*-tdTomato targeting construct²³, which contains the *T2A-tdTomato-BGHpA* cassette between the 5' (intron 3 and exon 4; 1,393 bp) and 3' (exon 4 and intron 4; 816 bp) targeting arms. The tdTomato sequence was replaced by the creERT2 sequence to obtain a *Hif-creERT2* targeting construct. The resulting plasmid (10 ng μ l^{−1} in water), Cas9 protein (50 ng μ l^{−1}; Thermo Fisher Scientific), crRNA (5'-AGGC ACAGGGCCCCUGUAAGAguuuuagaggcuaugcuguuuug-3'; 50 ng μ l^{−1}), and tracrRNA (50 ng μ l^{−1}; FASMAC) were injected into C57BL/6J fertilized eggs. *Hif*^{creERT2} mice were genotyped by PCR amplification using the following primers: forward (5'-TAGTTGCCAGCCATCTGTTG-3') and reverse (5'-TCCCATTCTGAGATACACCAAGTG-3'). The annealing location of the reverse primer was designed to be outside the homology arm. The wild-type *Hif* allele was detected by PCR using forward (5'-CAGGAGGTGCTGATTAAAG-3') and reverse (5'-TCCCATTCTGAGATACACCAAG TG-3') primers.

Generation of the *Evi1*^{creERT2} knock-in mouse

Evi1^{creERT2} mice were generated by inserting *Evi1* cDNA (exon 9–15)-*P2A-creERT2* gene fusion into exon 9, similar to the *Evi1*^{GFP} knock-in strategy³⁰. The targeting vector was generated by modifying the *Evi1-mVenus* targeting construct, prepared by gene synthesis (Genewiz). The synthesized part of the *Evi1-mVenus* construct is as follows: 5' arm (intron 8; 379 bp)-exon9-15-*P2A-mVenus-BGHpA*-3' arm (intron 9; 502 bp). *Evi1* sequence information was obtained from Ensembl (Transcript ID, ENSMUST00000108270.9). The mVenus sequence was replaced by the creERT2 sequences to obtain the *Evi1-creERT2* targeting construct. The resulting plasmid (10 ng μ l^{−1} in water), Cas9 protein (50 ng μ l^{−1}; Thermo Fisher Scientific), and crRNA (5'-AGGGGAGAUUCCAGCUGGUuuuuuagaggcuaugcuguuuug-3'; 2.5 μ M) and tracrRNA (2.5 μ M; FASMAC) were injected into C57BL/6J fertilized eggs. Generated *Evi1*^{creERT2} mice were genotyped by PCR amplification using the following primers: forward (5'-AC CAACTGGACACATGACAGAACAT-3') and reverse (5'-GCCATT

CATCCTCTTCCATGTTC-3' for knock-in allele) (5'-GGCTGCCCTACCGATCTTGTG-3' for the wild-type allele).

Generation of the *ROSA*^{Evi1-IRES-GFP} knock-in mouse

ROSA^{Evi1-IRES-GFP} mice were generated by inserting the *Evi1* cDNA-*IRES-EGFP* fusion gene into intron 1 of the *ROSA26* locus. The targeting vector was generated by inserting *Evi1* cDNA (Addgene #101858) into the STOP-eGFP-*ROSA26*TV plasmid (Addgene #11739). For the combinational use of the CRISPR–Cas system, two sets of single guide RNA oligonucleotides (5'-caccTGCGGGAGTCTTCTGGGC-3' and 5'-aaacGCCAGAAGACTCCGCCAc-3' for pX335-Rosa26-3, and 5'-caccGACTGGAGTTGCAGATCAGC-3' and 5'-aaacCGTGATCTGCAACTCCAGTC-3' for pX335-Rosa26-4) were cloned into the *BbsI*-digested pX335-U6-Chimeric_BB-CBh-hSpCas9n(D10A) plasmid (Addgene #42335). The resulting plasmids, the targeting vector, pX335-Rosa26-3 and pX335-Rosa26-4, were introduced into 6NK7 embryonic stem (ES) cells⁴⁷. The G418-resistant ES clones were screened for homologous recombination with the *ROSA26* locus by PCR using the following primers: 5' junction forward (5'-CTCAGAGGCCTCGGCTAGGTAGGGATCG-3'), reverse (5'-GGTTCTTTGTCAAGACCGACCTGT-3'); 3' junction forward (5'-GTCTATATCATGGCCGACAAGCAGAAGA-3'), reverse (5'-GTAAGTCATGCCCTCTTGGTACACCAC-3'); *Evi1* cDNA forward (5'-GGCGCGCCACCATGAAGAGTGAAGAGGACCCGCAC-3'), reverse (5'-GGCGCCCTACATGGCTATGGACTGGATGGCACTG-3'). Chimeric mice were generated by aggregation (host ICR) of recombinant ES cells. Chimeric males were mated with C57BL/6J mice to obtain germline transmission. Generated *ROSA*^{Evi1-IRES-GFP} mice were genotyped by PCR amplification using the following primers: *ROSA* locus forward (5'-AAAGTCGCTCTGAGTTGTTAT-3'), reverse (5'-AAGACCGCGAAGAGTTGTC-3' for KI allele, 5'-GGAGC GGGAGAAATGGATATG for the wild-type allele); *Evi1* cDNA forward (5'-CTGAGGAGAGGAATAACAGTGTG-3') and reverse (5'-ACACT GCTGTGGATGTGCTTG-3').

Generation of the *ROSA*^{CAG-Evi1-IRES-GFP} knock-in mouse

ROSA^{CAG-Evi1-IRES-GFP} mice were generated by inserting the *Evi1* cDNA-*IRES-EGFP* fusion gene into intron 1 of the *ROSA26* locus. The targeting vector was generated by inserting *Evi1* cDNA-*IRES-EGFP* into the Ai9 plasmid (Addgene #22799). The *Evi1* cDNA-*IRES-EGFP* fragment was amplified from our targeting vector of *ROSA*^{Evi1-IRES-GFP} by PCR using the following primers: forward (5'-CAGACGCGTGCGCCACCATGAAGAGTGAAGAG-3'), reverse (5'-cttacgcgttaTTACTTGTACAGCTCGTCCATGC-3'). For the combinational use of the CRISPR–Cas system, two sets of single guide RNA oligonucleotides (5'-caccTGCGGGAGTCTTCTGGGC-3' and 5'-aaacGCCAGAAGACTCCGCCAc-3' for pX335-Rosa26-3, and 5'-caccGACTGGAGTTGCAGATCAGC-3' and 5'-aaacCGTGATCTGCAACTCCAGTC-3' for pX335-Rosa26-4) were cloned into the *BbsI*-digested pX335-U6-Chimeric_BB-CBh-hSpCas9n(D10A) plasmid (Addgene #42335). The resulting plasmids, the targeting vector, pX335-Rosa26-3 and pX335-Rosa26-4, were introduced into 6NK7 ES cells⁴⁷. The G418-resistant ES clones were screened for homologous recombination with the *ROSA26* locus by PCR using the following primers: 5' junction forward (5'-CTCAGAGGCCTCGGCTAGGTAGGGATCG-3'), reverse (5'-CATTTACCGTAAGTTATGTAACCGGAACTC-3'); 3' junction forward (5'-CATGCCCTCTATCGCCTTCTTGAC-3'), reverse (5'-TGTTGAGGGCAATCTGGGAAG-3'); *Evi1* cDNA forward (5'-CTG AGGAGAGGAATAACAGTGTG-3'), reverse (5'-ACACTGCTGTGGATGTGCTTG-3'). Chimeric mice were generated by aggregation (host ICR) of recombinant ES cells. Chimeric males were mated with C57BL/6J mice to obtain germline transmission. Generated *ROSA*^{CAG-Evi1-IRES-GFP} mice were genotyped by PCR amplification using the following primers: *ROSA* locus forward (5'-CTCAGAGGCCTCGGCTAGGTAGGGATCG-3'), reverse (5'-CATTTACCGTAAGTTATGTAACCGGAACTC-3') for KI allele, forward (5'-AAAGTCGCTCTGAGTTGTTAT-3'), reverse

Article

(5'-GGAGCGGGAGAAATGGATATG) for the wild-type allele; *Evi1* cDNA forward (5'-CTGAGGAGAGGGAATACAAGTGTG-3') and reverse (5'-ACACTGCTGTGGATGTGCTTG-3').

Whole-mount immunostaining of embryos

Whole-mount immunostaining was performed as described previously⁴⁸. In brief, embryos were fixed for 20 to 30 min in 2% paraformaldehyde diluted in phosphate-buffered saline (PBS) on ice, and dehydrated in graded concentrations of methanol/PBS (50%, 100%; 10 min each). The yolk sac, head, limb buds and lateral body wall were removed in 100% methanol to stain around the dorsal aorta. After pre-incubation with PBS-MT (PBS containing 0.4% Triton X-100 and 1% skim milk) for at least 1 h, samples were incubated overnight with primary antibody diluted in PBS-MT. Samples were washed three times in PBS-MT throughout the next day (2 to 3 h per wash). Secondary antibodies were diluted in PBS-MT, and samples were incubated overnight. Primary antibodies were to KIT (rat, 2B8; BD Biosciences, 1:500), CD31 (rat, MEC13.3; BD Biosciences, 1:500), KIT (goat; RnD Systems, 1:2,000), CD31 (hamster, 2H8; Merck, 1:1,000), GFP (rabbit; MBL, 1:2,000), RFP (rabbit; Rockland Immunochemicals, 1:1,000). Secondary antibodies were donkey anti-rat IgG-Cy3 (Jackson ImmunoResearch, 1:5,000), donkey anti-rat IgG-Alexa Fluor 647 (Invitrogen, 1:5,000), goat anti-rabbit IgG-Alexa Fluor 647 (Invitrogen, 1:5,000), donkey anti-rabbit IgG-Cy3 (Jackson ImmunoResearch, 1:5,000), goat anti-hamster IgG-Alexa Fluor 488 (Jackson ImmunoResearch, 1:5,000), goat anti-hamster IgG-Alexa Fluor 647 (Jackson ImmunoResearch, 1:5,000) and donkey anti-goat IgG-Alexa Fluor 488 (Invitrogen, 1:5,000). Nuclei were visualized with Hoechst 33258 (Invitrogen).

Confocal microscopy and image analysis

Immunostained caudal half region and yolk sac were mounted in a 1:2 mix of benzyl alcohol and benzyl benzoate (BABB) to increase tissue transparency, and then analysed by confocal microscopy (Olympus FV-1200 equipped with GaAsP PMT detectors, UPLSAPO 20×/NA 0.75 and FV10-ASW software or Nikon A1 HD25 equipped with Plan Apo VC 20×/0.75, Plan Fluor 10×/0.30 and NIS-Elements AR software). Tile-scanning was performed using a motor-driven x–y scanning stage to observe large areas. Three-dimensional reconstructions were generated from z-stacks with Olympus FLUOVIEW software or Imaris software (Bitplane). Among the cells embedded in the endothelial cell layer, cells with a flattened shape were defined as endothelial cells and those with a hemispherical shape as HCCs.

Cell preparation and flow cytometry

Single-cell suspensions were prepared by treating tissues with collagenase (0.125% in PBS/10% fetal calf serum (FCS)/1% penicillin/streptomycin) for 1 h at 37 °C. Bone marrow cells were prepared by crushing the bones using a mortar. Cell number was counted using a TC20 automated cell counter (Bio-Rad). Cells were stained with fluorescence-conjugated antibodies: KIT (2B8, BV421; BioLegend, 1:200), KIT (2B8, PE-Cy7; BioLegend, 1:400), KIT (2B8, APC; BioLegend, 1:200), CD31 (MEC13.3, FITC; BD Biosciences, 1:100), CD31 (MEC13.3, BV421; BD Biosciences, 1:100), CD45 (30-F11, APC-Cy7; BD Biosciences, 1:200), CD45 (30-F11, BV510; BD Biosciences, 1:100), SCA-1(D7, PE-Cy7; BioLegend, 1:400), CD150 (TC15-12F12.2, BV421; BioLegend, 1:50), CD48 (HM48-1, FITC; BioLegend, 1:50), CD48 (HM48-1, PE; BioLegend, 1:200), CD41 (MWReg30, PerCP-eFluor710; eBioscience, 1:100), CD41 (MWReg30, APC-Cy7; BioLegend, 1:100), CD16/32 (93, APC; BioLegend, 1:100), CD16/32 (93, APC-Cy7; BioLegend, 1:100), CD34 (RAM34, FITC, eBioscience, 1:50), CD34 (RAM34, AlexaFluor647, BD Biosciences, 1:25), EPCR (eBio1560, APC; eBioscience, 1:150), TER119 (TER-119, FITC; BioLegend, 1:200), TER119 (TER-119, PerCP-Cy5.5; BioLegend, 1:100), CD3e (IgG2C11, PerCP-Cy5.5; BioLegend, 1:50), CD4 (RM4-5, PerCP-Cy5.5; BioLegend, 1:100), CD4 (RM4-5, APC; BioLegend, 1:100), CD4 (RM4-5, APC-Cy7; BioLegend, 1:100), CD8a (53-6.7, PerCP-Cy5.5; BioLegend,

1:100), CD8a (53-6.7, APC; BioLegend, 1:100), CD8a (53-6.7, APC-Cy7; BioLegend, 1:100), B220 (RA3-6B2, PerCP-Cy5.5; BioLegend, 1:50), B220 (RA3-6B2, PE-Cy7; BioLegend, 1:200), Gr-1(RB6-8C5, PE; BioLegend, 1:200), Gr-1(RB6-8C5, PerCP-Cy5.5; BioLegend, 1:200), Mac-1(M1/70, PerCP-Cy5.5; BioLegend, 1:100), Mac-1(M1/70, FITC; BD Biosciences, 1:100), Mac-1(M1/70, PE; BioLegend, 1:200), CD45.1(A20, FITC; BioLegend, 1:400), CD45.2 (104, APC; BioLegend, 1:200), Flt3 (A2F10, APC; BioLegend, 1:100), IL7Ra (A7R34, BV421; BioLegend, 1:20), CD86 (GL1, APC; BD Biosciences, 1:50). Cells were analysed by FACS ArialIII, FACS Canto II, or FACSymphony (BD Biosciences). Data were analysed using FlowJo software (Tree Star).

Combinations of cell surface markers and transcription factors were used to identify the following populations: HSC (CD150⁺CD48⁺KIT⁺SCA-1⁻Lin⁻), ST-HSC (CD150⁺CD48⁺KIT⁺SCA-1⁻Lin⁻), MPP (CD150⁺CD48⁺KIT⁺SCA-1⁻Lin⁻), CMP (CD34⁺FcyR⁺KIT⁺SCA-1⁻Lin⁻), GMP (CD34⁺FcyR⁺KIT⁺SCA-1⁻Lin⁻), MEP (CD34⁺FcyR⁺KIT⁺SCA-1⁻Lin⁻), EMP (KIT⁺CD41⁺CD16/32⁺), LMP (KIT⁺CD45⁺IL7R^aFlt3⁺Lin⁻), HCC (HLF⁺KIT⁺), EC (CD31⁺CD45⁺CD41⁻), erythrocytes (Ter119⁺CD41⁻), platelets (CD41⁺Ter119⁻), myeloid cells (CD11b⁺Gr-1⁺), B cell (B220⁺CD4⁺CD8⁻CD11b⁻) and T cell (CD4⁺B220⁺CD11b⁻). Mac-1 was only used in the lineage cocktail for adult bone marrow.

scRNA-seq

The middle segment of the dorsal aorta and a lobe of the fetal liver were isolated from E10.5 (35 sp) and E11.5 (45 sp) C57BL/6N mouse embryos. Tissues were dissociated using 1 mg ml⁻¹ collagenase–dispase (Roche Diagnostics) for 5 min at 37 °C and then 0.25% trypsin-EDTA (Thermo Fisher Scientific) for 7 min at 37 °C. Cells were washed with 1% BSA/HBSS and with 1% BSA/PBS. Cells were then resuspended in 0.04% BSA/PBS, filtered through a nylon mesh, and evaluated for cell number and viability (>90%) using a Countess automated cell counter (Thermo Fisher Scientific). A total of 7,000 cells each from E10.5 and E11.5 were applied to a Chromium Controller (10x Genomics). Chromium Single Cell 3' v3.1 kit (10x Genomics) was used to generate oligo(dT)-primed cDNA libraries, which were then sequenced using an Illumina HiSeqX.

Raw sequence data were processed using the cellranger count command of Cell Ranger (v5.0.0; 10x Genomics), with the 2 datasets (E10.5 and E11.5) then integrated using the cellranger aggr command. All subsequent analyses were performed in the R environment (v3.6.1 (x64)). The Seurat package (v4.0.0) was used for analyses of quality control, data normalization, data scaling, and visualization^{49,50}. In the first round of quality control, the following cells were excluded: cells with < 250 gene expression per cell, < 1,000 unique molecular identifier (UMI) counts per cell, < 0.76 log₁₀(genes detected)/log₁₀(UMI count), or cells with mitochondrial genes accounting for more than 35% of all genes^{51–53}. Principal component analysis (PCA) was performed on the remaining cells, and the results were visualized with JackStrawPlot; a dimension value of 76 was used for subsequent analyses. Clustering was done using FindClusters with a resolution of 2.0. To visualize these data, uniform manifold approximation and projection for dimension reduction (UMAP) plots were generated using the uwot package (v0.1.10). The UMAP coordinates, Seurat cluster coordinates, and cluster-specific markers were exported as csv files for confirmation analysis using Loupe Brower software (10x Genomics). Fifty clusters were found to have formed, of which 11 clusters were determined to be dying cells that escaped the filtering parameters because they lacked specific marker genes, had few mitochondrial genes, or had a relatively small number of features. These 11 clusters were removed. We then performed a second round of quality control, excluding cells with < 620 gene expression per cell, < 1,000 UMI count per cell, < 0.76 log₁₀(genes detected)/log₁₀(UMI counts), or cells with mitochondrial genes accounting for more than 35% of all genes. PCA was performed on the remaining cells, and the results were visualized with JackStrawPlot; a dimension value of 73 was used for subsequent analyses. Clustering was done as above, with 45 clusters confirmed. Of these, two clusters were determined to be dying

cells that escaped filtering, and were removed. In the third round of quality control, cells with < 620 gene expression per cell, <1,000 UMI count per cell, <0.78 log₁₀(genes detected)/log₁₀(UMI counts), or cells with mitochondrial genes accounting for more than 35% of all genes were excluded. PCA was performed, and the results were visualized with JackStrawPlot with a dimension value of 78. Clustering was done using FindClusters with a resolution of 0.1, with a final 15 clusters confirmed. The final dataset contained 20,813 genes and 13,193 cells (E10.5, 6,608 cells; E11.5, 6,585 cells). Cell types were annotated semi-manually based on the expression pattern of cell-specific markers (Supplementary Table 1). To identify genes specifically expressed in each cluster for the determination of cell types, we performed differential gene expression analysis using Loupe Browser software (10x Genomics). Results with an adjusted *P*-value < 0.1 (using Benjamini–Hochberg correction for multiple tests) were considered significant. The pre-HSPC gene expression heat map was produced using the heatmap.2 function from the gplots R package (v3.1.1)⁵⁴. The gene expression data were normalized and scaled using the Seurat package (v4.0.4)⁵⁵. Hierarchical clustering was carried out using the *hclust* R function with the ward.D2 method.

Analysis of scRNA-seq data

SPRING visualization in Extended Data Fig. 4h–k was obtained using the interactive website (<https://gottgens-lab.stemcells.cam.ac.uk/DZIERZAK/>). To generate the pre-HSPC gene expression heat map, scRNA-seq datasets of mouse *Gata2*-expressing intra-aortic HCCs (the Vink et al.⁵⁶ dataset; GSE143637) and mouse EHT process-related cells (the Fadlullah et al.⁵⁷ dataset; GSE150412) were analysed using the R package (v4.1.2 (×64)). The Seurat package (v4.1.0) was used for analyses of quality control, data normalization, data scaling and visualization^{49,50}. In the quality control of the Vink et al. dataset, the following cells were excluded: cells with < 5,000 genes expressed per cell, <80,000 UMI count per cell, >0.78 log₁₀(genes detected)/log₁₀(UMI counts), or cells with mitochondrial genes accounting for more than 10% of all genes^{51–53}. PCA was performed on the remaining cells, and the results were visualized by JackStrawPlot; a dimension value of 100 was used for subsequent analyses. Clustering was done using FindClusters command with a resolution of 0.5, and a final 5 clusters were confirmed. The final dataset contained 24,182 genes and 1,085 cells. In the quality control of the Fadlullah et al. dataset, the following cells were excluded: cells with <1,800 gene expression per cell, <80,000 UMI count per cell, >0.75 log₁₀(genes detected)/log₁₀(UMI counts), or cells with mitochondrial genes accounting for more than 20% of all genes^{51–53}. PCA was performed on the remaining cells, and the results were visualized with JackStrawPlot; a dimension value of 100 was used for subsequent analyses. Clustering was done using FindClusters with a resolution of 0.5, and a final 8 clusters were confirmed. The final dataset contained 18,796 genes (*Il7r* was not included) and 1,258 cells. To visualize these data, UMAP plots were generated using the uwot package (v0.1.11). The pre-HSPCs (HLF⁺KIT⁺ cells; 52 cells from the Vink et al. dataset and 27 cells from the Fadlullah et al. dataset) were extracted, and hierarchical clustering was carried out using the pheatmap package (v1.0.12).

RNA sequencing

Random displacement amplification sequencing (RamDA-seq) was performed, as previously described⁵⁸. In brief, using 100 sorted cells, first-strand cDNA was synthesized using PrimeScript RT reagent Kit (TAKARA) and not-so random primers. After first-strand synthesis, the second strand was synthesized using Klenow Fragments (3'–5' exo-) (New England Biolabs) and complementary chains of not-so random primers. The double-stranded cDNA was purified, and the library for RNA-seq was prepared and amplified by Nextera XT DNA sample Prep Kit (Illumina), according to the manufacturer's instructions. This prepared library was sequenced on a Next-Seq system (Illumina). Each obtained read was mapped to the reference sequence GRChm38/mm10 using HISAT2. TPM and reads count for each gene were calculated using

StringTie. Differentially expressed genes were identified with edgeR. Heat maps were generated using Prism 8 (v8.4.3, GraphPad). Gene set enrichment analysis (GSEA) was performed using GSEA v4.1.0 (<http://www.broadinstitute.org/gsea/>). Gene sets were obtained from Gazit et al.⁵⁹. PCA was performed using the prcomp R function with the 'center' and 'scale' parameters. Genes with zero TPM variance across samples were removed and TPM values were log transformed (log₂(TPM+1)) before plotting the PCA.

Blood cell analysis

Peripheral blood was collected by retro-orbital bleeding under anaesthesia, and complete blood cell counts were performed using a poch-100i V Diff automated haematology analyser (Sysmex).

Transplantation

GFP⁺ HSCs, sorted from *Tie2-cre::ROSA*^{Evi1-IRES-GFP} fetal liver, and HSPC fractions (HSC, ST-HSC, and MPP) sorted from wild-type fetal liver were co-injected intravenously with competitor cells (2 × 10⁵ spleen cells for GFP⁺ HSCs or 2 × 10⁵ bone marrow cells for HSPC fractions) into 9.0 Gy (4.5 Gy, each of two doses)-irradiated mice. Repopulation was assayed at 4, 8, 12 and 16 weeks after transplantation. Peripheral blood was collected by retro-orbital bleeding under anaesthesia. Cells were analysed by FACS Canto II or FACSymphony (BD Biosciences).

Statistics and reproducibility

Two-sided Student's *t*-test (Figs. 3b,d,f and 4f,g and Extended Data Figs. 2e–g, 5c, 6b,c, 7c, 8a–c, 9c,d,j and 10a), one-way ANOVA with Tukey–Kramer test (Fig. 2b,h and Extended Data Fig. 9e,f) and one-way ANOVA with Dunnett's test (Fig. 4e) were used to determine differences between datasets with Prism 8 software (v8.4.3, GraphPad). Data are mean ± s.d. Two-sided *P* values are shown (**P* < 0.05, ***P* < 0.01, ****P* < 0.001, *****P* < 0.0001, NS: not significant). Representative micrographs from at least two biological replicates are shown (see Supplementary Table 2 for the detailed sample size information).

Reporting summary

Further information on research design is available in the Nature Research Reporting Summary linked to this article.

Data availability

All RNA-seq data were deposited in the Gene Expression Omnibus under accessions GSE167932 (E10.5 and E11.5 scRNA-seq), GSE168054 (E10.5 bulk RNA-seq) and GSE190011 (E14.5 bulk RNA-seq). Source data are provided with this paper.

41. Matsuo, J. et al. Identification of stem cells in the epithelium of the stomach corpus and antrum of mice. *Gastroenterology* **152**, 218–231.e14 (2017).
42. Okabe, K. et al. Neurons limit angiogenesis by titrating VEGF in retina. *Cell* **159**, 584–596 (2014).
43. Madisen, L. et al. A robust and high-throughput Cre reporting and characterization system for the whole mouse brain. *Nat. Neurosci.* **13**, 133–140 (2010).
44. Srinivas, S. et al. Cre reporter strains produced by targeted insertion of EYFP and ECFP into the ROSA26 locus. *BMC Dev. Biol.* **1**, 4 (2001).
45. de Boer, J. et al. Transgenic mice with hematopoietic and lymphoid specific expression of Cre. *Eur. J. Immunol.* **33**, 314–325 (2003).
46. Kisanuki, Y. Y. et al. Tie2-Cre transgenic mice: a new model for endothelial cell-lineage analysis in vivo. *Dev. Biol.* **230**, 230–242 (2001).
47. Ishikawa, E. et al. Protein kinase D regulates positive selection of CD4⁺ thymocytes through phosphorylation of SHP-1. *Nat. Commun.* **7**, 12756 (2016).
48. Yokomizo, T. et al. Whole-mount three-dimensional imaging of internally localized immunostained cells within mouse embryos. *Nat. Protoc.* **7**, 421–431 (2012).
49. Butler, A., Hoffman, P., Smibert, P., Papalexi, E. & Satija, R. Integrating single-cell transcriptomic data across different conditions, technologies, and species. *Nat. Biotechnol.* **36**, 411–420 (2018).
50. Stuart, T. et al. Comprehensive integration of single-cell data. *Cell* **177**, 1888–1902.e21 (2019).
51. Chen, J. et al. An in situ atlas of mitochondrial DNA in mammalian tissues reveals high content in stem and proliferative compartments. *Am. J. Pathol.* **190**, 1565–1579 (2020).
52. Ransick, A. et al. Single-cell profiling reveals sex, lineage, and regional diversity in the mouse kidney. *Dev. Cell* **51**, 399–413.e7 (2019).

Article

53. Mercer, T. R. et al. The human mitochondrial transcriptome. *Cell* **146**, 645–658 (2011).
54. Warnes, G. R. et al. gplots: various R programming tools for plotting data. R package version 3.1.1 (2020).
55. Hao, Y. et al. Integrated analysis of multimodal single-cell data. *Cell* **184**, 3573–3587.e29 (2021).
56. Vink, C. S. et al. Iterative single-cell analyses define the transcriptome of the first functional hematopoietic stem cells. *Cell Rep.* **31**, 107627 (2020).
57. Fadullah, M. Z. H. et al. Murine AGM single-cell profiling identifies a continuum of hemogenic endothelium differentiation marked by ACE. *Blood* **139**, 343–356 (2022).
58. Hayashi, T. et al. Single-cell full-length total RNA sequencing uncovers dynamics of recursive splicing and enhancer RNAs. *Nat. Commun.* **9**, 619 (2018).
59. Gazit, R. et al. Transcriptome analysis identifies regulators of hematopoietic stem and progenitor cells. *Stem Cell Rep.* **1**, 266–280 (2013).
60. Perdigero, E. G. et al. The origin of tissue-resident macrophages: when an erythro-myeloid progenitor is an erythro-myeloid progenitor. *Immunity* **43**, 1023–1024 (2015).
61. Soares-da-Silva, F. et al. Yolk sac, but not hematopoietic stem cell-derived progenitors, sustain erythropoiesis throughout murine embryonic life. *J. Exp. Med.* **218**, e20201729 (2021).

Acknowledgements We thank E. Dzierzak for critical comments on this manuscript; and T. Umemoto, M. Kataoka and R. Koitabashi for assistance with RNA sequencing. This work was supported by JSPS Kakenhi Grant (20K08758, JP16H0627 (AdAMS) to T.Y. and 26221309 to T. Suda), SENSHIN Medical Research Foundation (to T.Y.), Takeda Science Foundation (to T.Y.).

Japanese Society of Hematology (to T.Y.), the Sumitomo Foundation (to T.Y.), the National Medical Research Council grant of Singapore Translational Research Investigator Award (NMRC/STA/R/0019/2014 to T. Suda) and the programme of the Inter-University Research Network for High Depth Omics, Institute of Molecular Embryology and Genetics, Kumamoto University (to S.M.-K. and M. Ogawa).

Author contributions T.Y. conceived the project, designed and performed the research, and wrote the manuscript. T.I. made the targeting constructs and performed whole-mount immunostaining. S.M.-K. and M. Ogawa performed the scRNA-seq analysis. C.Y.T. and M. Osato performed the bioinformatic analysis. N.T. and K.A. generated mouse lines. T. Sato, Y.K., M.K. and N.K. contributed analytical tools. T.Y., M. Osato and T. Suda participated in project planning.

Competing interests The authors declare no competing interests.

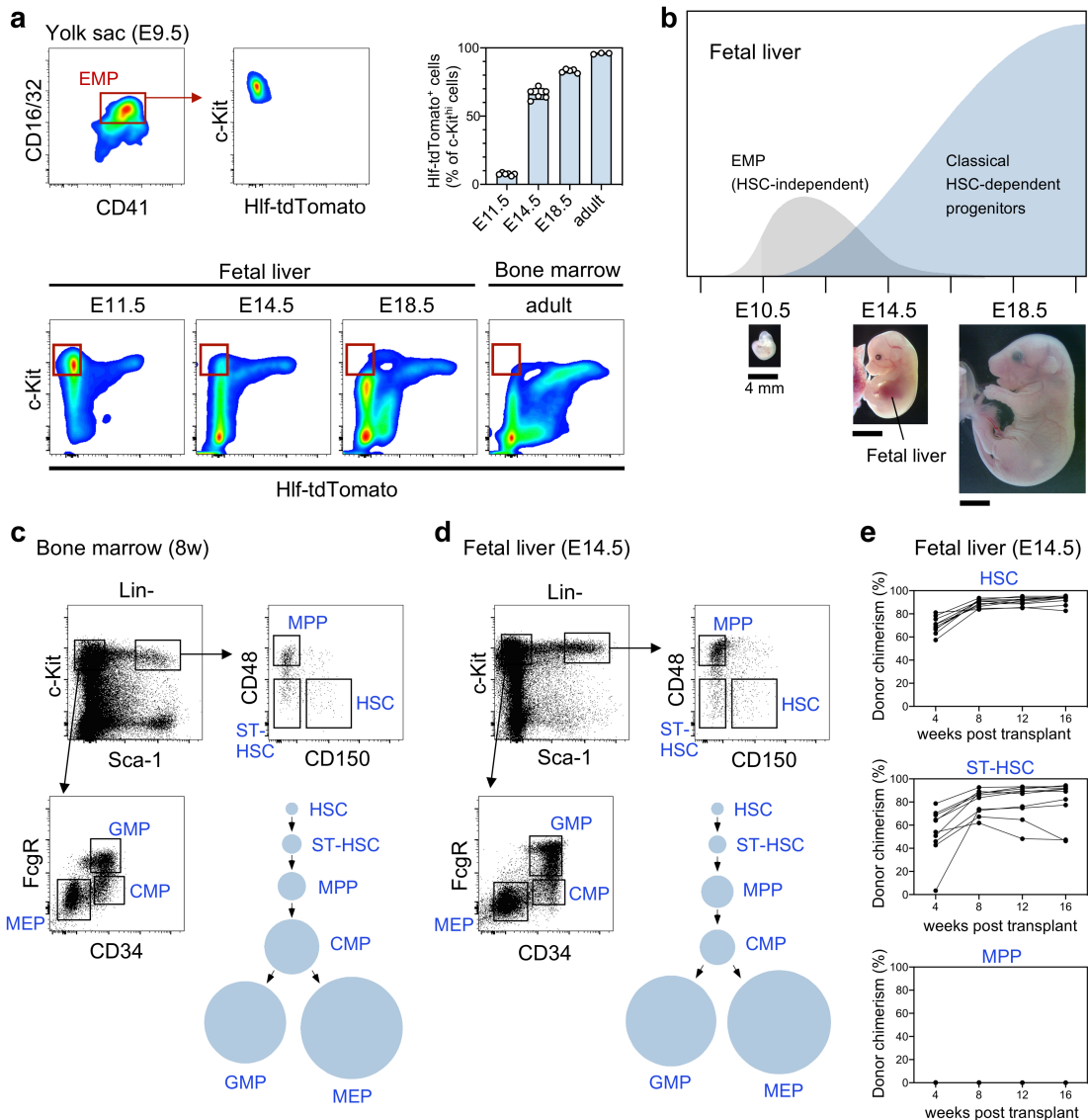
Additional information

Supplementary information The online version contains supplementary material available at <https://doi.org/10.1038/s41586-022-05203-0>.

Correspondence and requests for materials should be addressed to Tomomasa Yokomizo or Toshio Suda.

Peer review information *Nature* thanks Anna Bigas, Georges Lacaud and the other, anonymous, reviewer(s) for their contribution to the peer review of this work. Peer reviewer reports are available.

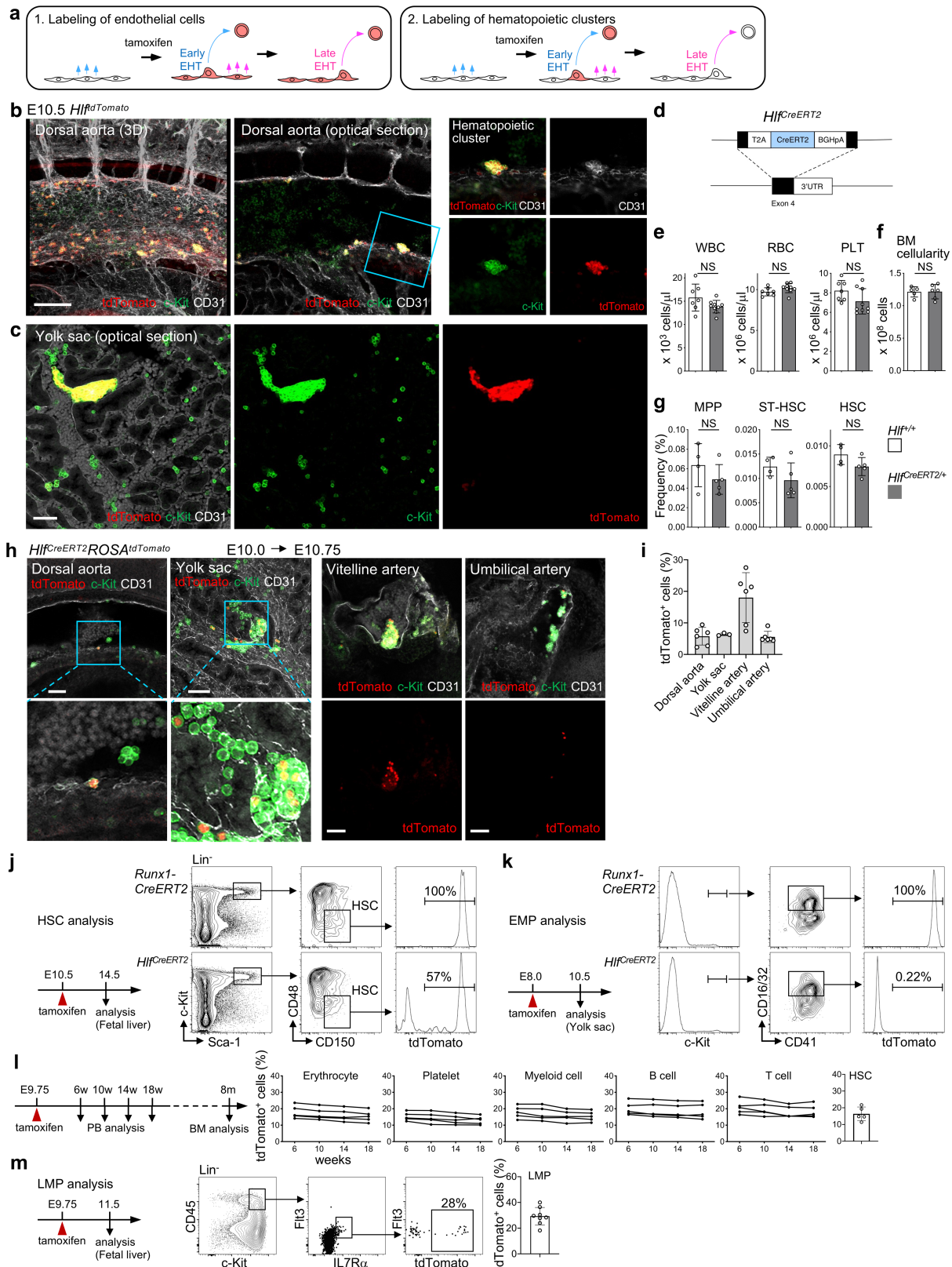
Reprints and permissions information is available at <http://www.nature.com/reprints>.



Extended Data Fig. 1 | Hematopoietic stem/progenitor cells in the late gestational fetal liver. **a**, Disappearance of EMPs at mid-late gestation. Since Hlf is not expressed in EMPs (red rectangle), EMPs and other progenitors can be distinguished by *Hlf-tdTomato* reporter²³. Top right, Frequency of Hlf-tdTomato⁺ cells in c-Kit^{hi} cells (E11.5, n = 6; E14.5, n = 6; E18.5, n = 5; adult, n = 3). **b**, Waves of hematopoietic progenitors in the fetal liver. Schematic is drawn based on previous reports^{24,60,61} and our data (**a**). At E14.5, most c-Kit⁺ progenitors in the fetal liver are classical HSC-dependent progenitors. **c**, Representative flow cytometry plots and hematopoietic stem/progenitor cell hierarchy in the bone

marrow. Circle size represents the population size of the defined fractions. **d**, Representative flow cytometry plots and hematopoietic stem/progenitor cell hierarchy in the fetal liver (E14.5). Relative population size of progenitor fractions is similar to that of bone marrow progenitors. The hematopoietic stem/progenitor cell hierarchy in the late gestational fetal liver is believed to be established through the differentiation of fetal HSCs (arrows in the hierarchy) in the standard model. **e**, Transplantation experiments. Irradiated mice were transplanted with 100 donor cells (HSC, ST-HSC, or MPP) sorted from E14.5 fetal liver. n = 10.

Article

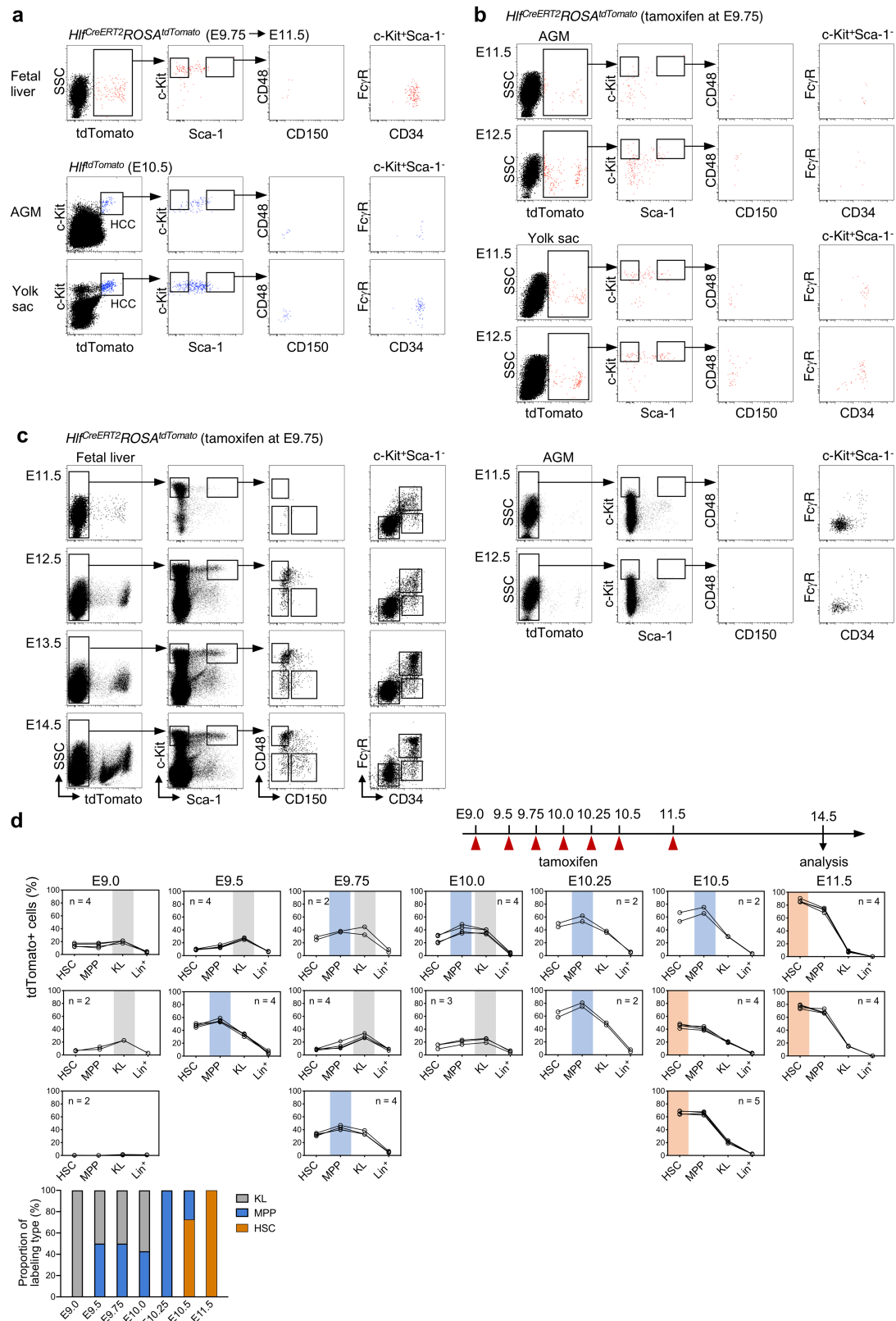


Extended Data Fig. 2 | See next page for caption.

Extended Data Fig. 2 | Generation and characterization of *Hlf*^{CreERT2} mice.

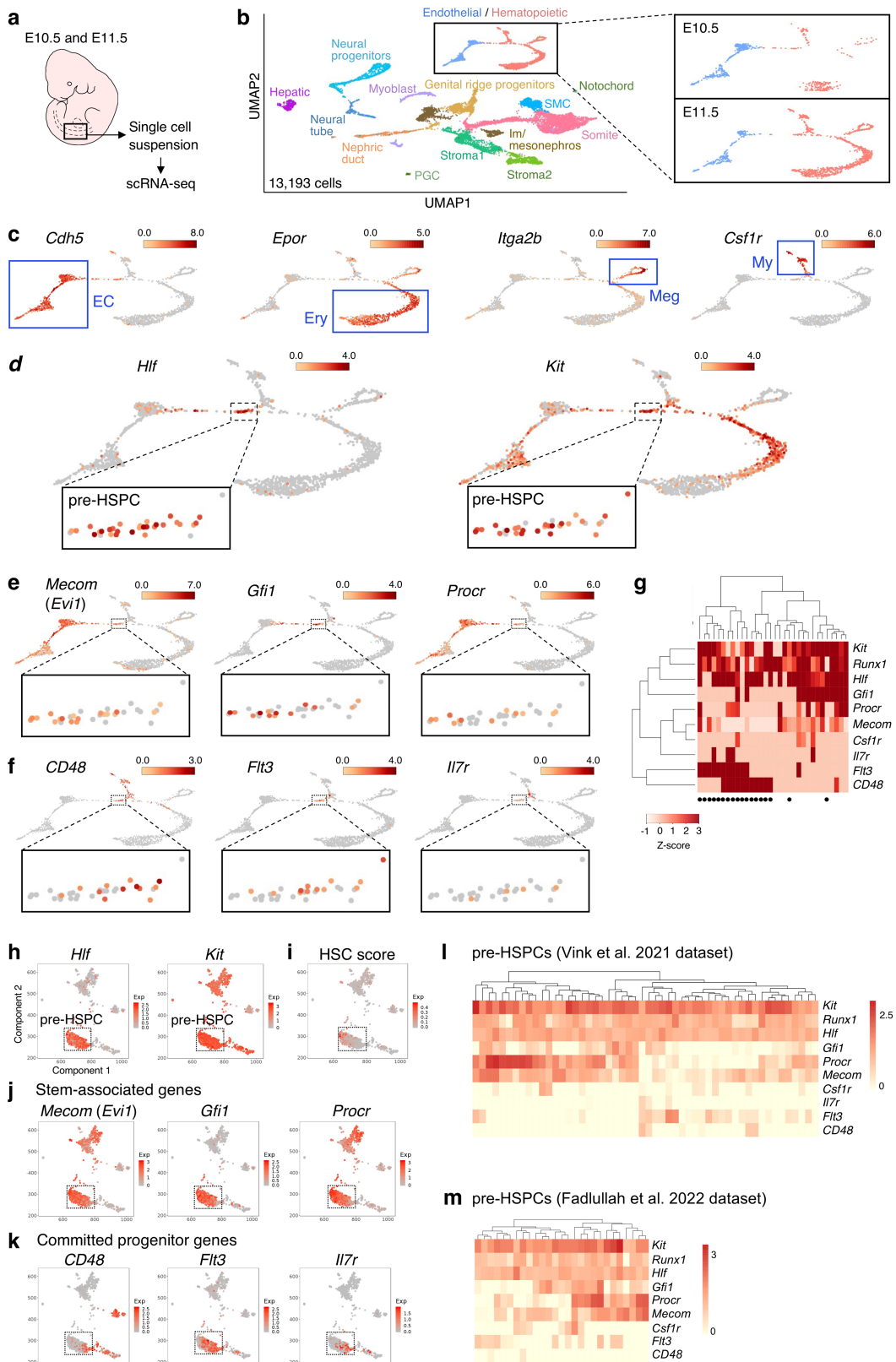
a, Experimental design for precursor labeling by CreERT2 lines. 1; Labeling of endothelial cells (e.g. *Runx1-CreERT2* and *VEcad-CreERT2*). Labeled endothelial cells may transform into hematopoietic cells at a later time, leading to the mixture of cells at various stage of maturation. 2; Labeling of hematopoietic clusters. EHT, endothelial-to-hematopoietic transition. **b**, Whole-mount immunostaining analysis of E10.5 (35 sp) *Hlf*^{tdTomato} embryos for tdTomato (red), c-Kit (green) and CD31 (white). Scale bar, 100 μ m. **c**, Whole-mount immunostaining analysis of E10.5 (33 sp) *Hlf*^{tdTomato} yolk sac for tdTomato (red), c-Kit (green) and CD31 (white). Scale bar, 50 μ m. **d**, Targeting strategy of the *Hlf*^{CreERT2} mouse. **e**, White blood cell (WBC), red blood cell (RBC), and platelet (PLT) fractions in the blood of adult *Hlf*^{+/+} and *Hlf*^{CreERT2/+} mice (*Hlf*^{+/+} mice, n = 7; *Hlf*^{CreERT2/+} mice, n = 9). **f**, Bone marrow (BM) cellularity (*Hlf*^{+/+} mice, n = 5; *Hlf*^{CreERT2/+} mice, n = 6). **g**, HSC and progenitor fractions in *Hlf*^{CreERT2/+} mice

(*Hlf*^{+/+} mice, n = 4; *Hlf*^{CreERT2/+} mice, n = 5). **h**, Whole-mount immunostaining analysis of E10.75 (tamoxifen at E10.0) *Hlf*^{CreERT2}*ROSA*^{tdTomato} embryos. Scale bars, 50 μ m. **i**, Frequency of tdTomato⁺ cells in c-Kit⁺ cells (Dorsal aorta, n = 6; Yolk sac, n = 3; Vitelline artery, n = 6; Umbilical artery, n = 6). **j**, HSC analysis. *Hlf*^{CreERT2}*ROSA*^{tdTomato} embryos were administered with tamoxifen at E10.5 and were analyzed at E14.5. **k**, EMP analysis. *Hlf*^{CreERT2}*ROSA*^{tdTomato} embryos were administered with tamoxifen at E8.0 and were analyzed at E10.5. **l**, Contribution of *Hlf*^{CreERT2}-labeled cells to adult hematopoiesis. *Hlf*^{CreERT2}*ROSA*^{tdTomato} embryos were administered with tamoxifen at E9.75. n = 5. **m**, Lympho-myeloid progenitor (LMP) analysis. *Hlf*^{CreERT2}*ROSA*^{tdTomato} embryos were administered with tamoxifen at E9.75 and were analyzed at E11.5. n = 8. All error bars represent means \pm SD. Statistical analysis was performed using two-sided unpaired Student's *t*-test (e–g).



Extended Data Fig. 3 | Fate tracing of Hif⁺ cells. **a**, Phenotypic comparison between E10.5 Hif⁺ c-Kit⁺ hematopoietic cluster cells and *HifCreERT2*-labeled cells in E11.5 fetal livers (tamoxifen at E9.75). **b**, Representative flow cytometry plots of *HifCreERT2*-labeled cells in the AGM and yolk sac (red dots). **c**, Representative flow cytometry plots of tdTomato⁺ fraction in the fetal liver and AGM of *HifCreERT2/ROSA^{tdTomato}* embryos. **d**, Top, Schematic of tamoxifen treatment and

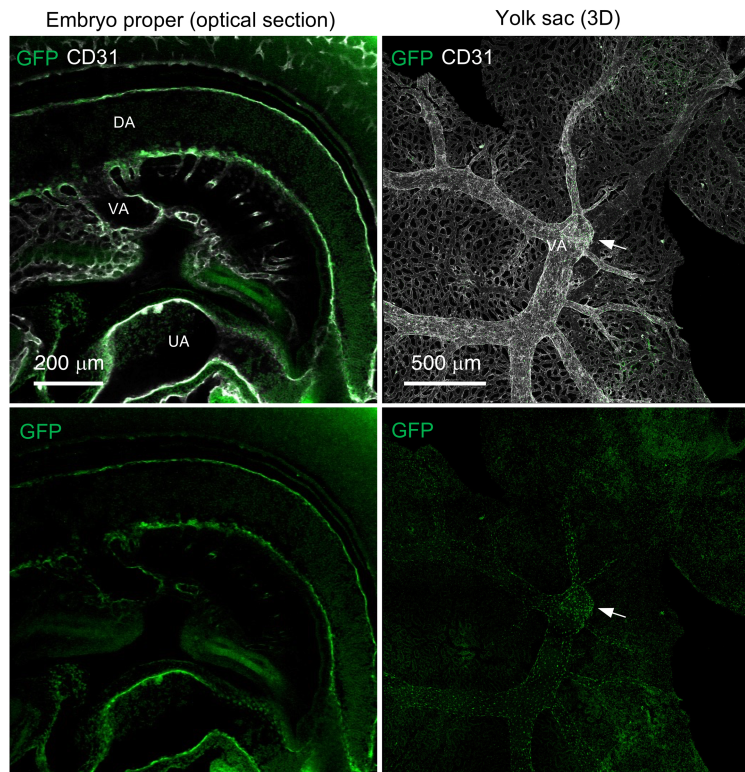
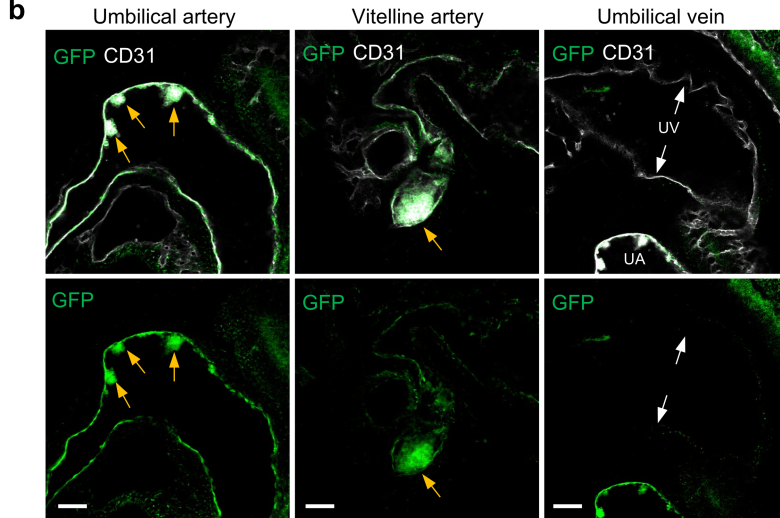
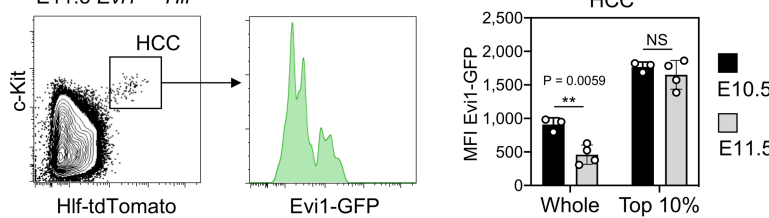
analysis. Middle, Lineage tracing of Hif⁺ cells. *HifCreERT2/ROSA^{tdTomato}* embryos were administered with tamoxifen at various stages (E9.0–11.5) and were analyzed at E14.5. Each graph represents data from one litter. The highest frequency population is shaded (KL, gray; MPP, blue; HSC, orange). Bottom, Proportion of dominant-cell types.



Extended Data Fig. 4 | See next page for caption.

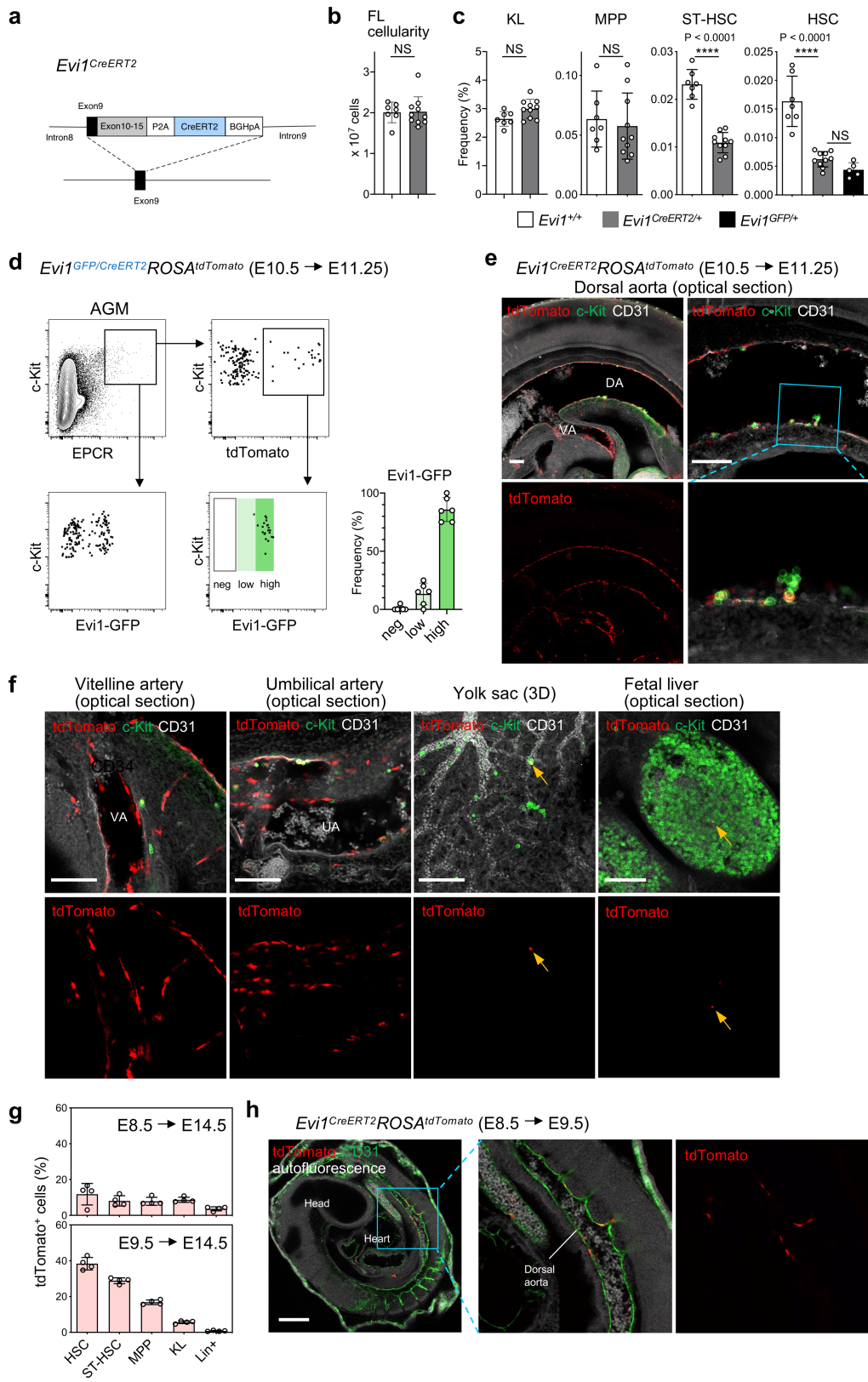
Article

Extended Data Fig. 4 | Heterogeneity within pre-HSPCs. **a**, Schematic of single-cell (sc)RNA-seq analysis. Middle segment of the dorsal aorta region and a lobe of the fetal liver were dissected to generate single cells from E10.5 and E11.5 embryos. **b**, Uniform manifold approximation and projection (UMAP) visualization of 13,193 cells isolated from the dorsal aorta and its surrounding tissues, including the fetal liver. Combined data from E10.5 (6,608 cells) and E11.5 (6,585 cells) are plotted. PGC, primordial germ cell; SMC, smooth muscle cell; Im, intermediate mesoderm. **c**, UMAP visualization of hematopoietic/endothelial clusters colored by representative lineage-specific genes (EC, endothelial cells; Ery, erythroid lineage; Meg, megakaryocytic lineage; My, myeloid lineage). **d**, Identification of Hlf^{hi}c-Kit^{hi} pre-HSPC population. **e**, UMAP visualization of stem-associated genes. **f**, UMAP visualization of committed hematopoietic marker genes. **g**, Hierarchical clustering of the Hlf^{hi}c-Kit^{hi} pre-HSPC population from E10.5 and E11.5 (marked by black circles) embryos. **h**, Identification of pre-HSPCs (Hlf^{hi}c-Kit^{hi}) in CD31^{hi}c-Kit^{hi}Gata2^{med} AGM single cells. SPRING visualization of selected genes from the interactive website (<https://gottgens-lab.stemcells.cam.ac.uk/DZIERZAK/>). **i**, HSC score. **j**, SPRING visualization of stem-associated genes. **k**, SPRING visualization of committed hematopoietic marker genes. **l**, Hierarchical clustering of the pre-HSPC population. Hlf^{hi}c-Kit^{hi} cells (n = 52) were extracted from the Vink et al. dataset (GSE143637). **m**, Hierarchical clustering of the pre-HSPC population. Hlf^{hi}c-Kit^{hi} cells (n = 27) were extracted from the Fadlullah et al. dataset (GSE150412).

a E10.5 *Evi1*^{GFP}**b****c E11.5 *Evi1*^{GFP}*Hlf*^{tdTomato}**

Extended Data Fig. 5 | *Evi1* expression in E10.5–11.5 embryos. **a, b,** Whole-mount immunostaining analysis of E10.5 (36 sp) *Evi1*^{GFP} embryos for GFP (green) and CD31 (white). **a,** Representative immunofluorescent images of the embryo proper and yolk sac. White arrows indicate the entrance of the yolk sac artery. GFP^{lo} cells are detected around this region. **b,** Representative immunofluorescent images of the umbilical artery, vitelline artery, and umbilical vein. Orange arrows indicate hematopoietic clusters. White arrows indicate the walls of the umbilical vein. Scale bars, 50 μm. DA, dorsal aorta;

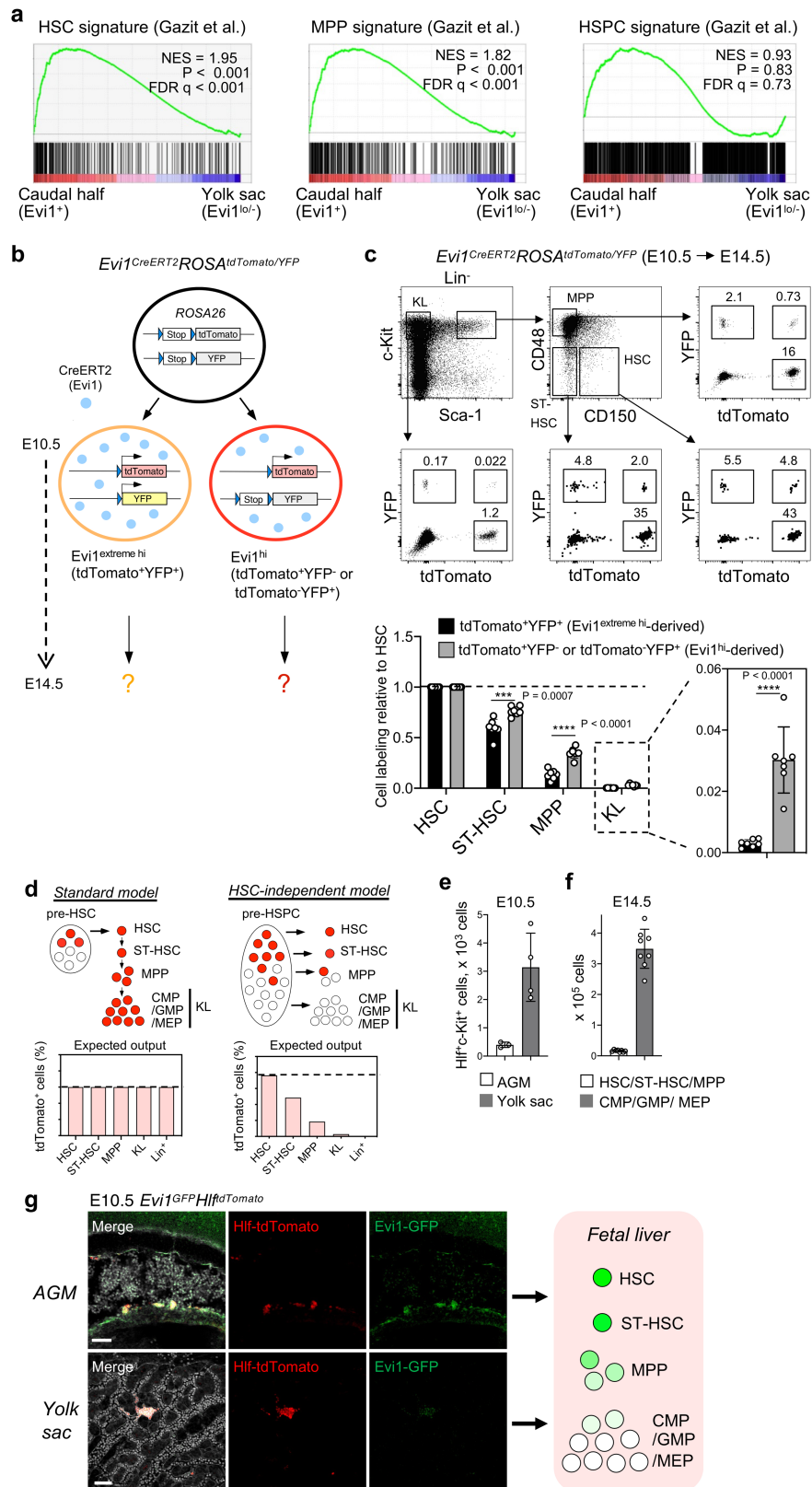
VA, vitelline artery; UA, umbilical artery; UV, umbilical vein. **c,** Flow cytometry analysis of *Evi1*-GFP expression in *Evi1*^{GFP/+}*Hlf*^{tdTomato/+} embryos. Left, Representative flow cytometry plots of the E11.5 *Evi1*^{GFP/+}*Hlf*^{tdTomato/+} AGM region. Right, Mean fluorescence intensity (MFI) of *Evi1*-GFP in the HCC fraction of the AGM region (E10.5, n = 3; E11.5, n = 4). HCC, hematopoietic cluster cell. All error bars represent means ± SD. Statistical analysis was performed using two-sided unpaired Student's *t*-test (**c**).



Extended Data Fig. 6 | See next page for caption.

Extended Data Fig. 6 | Fate tracing of Evi1^{hi} cells. **a**, Targeting strategy of the *Evi1*^{CreERT2} mouse. **b**, Fetal liver (FL) cellularity (*Evi1*^{+/+} mice, n = 7; *Evi1*^{CreERT2/+} mice, n = 10). **c**, HSC and progenitor fractions in *Evi1*^{CreERT2/+} (*Evi1*^{+/+} mice, n = 7; *Evi1*^{CreERT2/+} mice, n = 10; *Evi1*^{GFP/+} mice, n = 5). See Supplementary Discussion for HSC reduction in *Evi1*^{CreERT2} and *Evi1*^{GFP} embryos. **d**, Labeling of Evi1-GFP^{hi} cells by *Evi1*^{CreERT2}. *Evi1*^{CreERT2} mice were crossed with *Evi1*^{GFP}*ROSA*^{tdTomato} mice to obtain *Evi1*^{CreERT2/GFP}*ROSA*^{tdTomato} embryos (tamoxifen at E10.5). n = 6. **e**, Whole-mount immunostaining analysis of E11.25 (tamoxifen at E10.5) *Evi1*^{CreERT2}*ROSA*^{tdTomato} embryos. Labeled endothelial cells and hematopoietic clusters are observed in the dorsal aorta. Scale bars, 100 μm. **f**, Whole-mount immunostaining analysis

of E11.25 (tamoxifen at E10.5) *Evi1*^{CreERT2}*ROSA*^{tdTomato} embryos. In contrast to the vitelline and umbilical arteries, *tdTomato*⁺*c-Kit*⁺ cells are rarely observed in the yolk sac or fetal liver (orange arrows). Scale bars, 100 μm. **g**, Lineage tracing of Evi1⁺ cells. *Evi1*^{CreERT2}*ROSA*^{tdTomato} embryos were administered with tamoxifen at various stages (E8.5 and E9.5) and were analyzed at E14.5 (E8.5, n = 4; E9.5, n = 4). **h**, Whole-mount immunostaining analysis of E9.5 (tamoxifen at E8.5) *Evi1*^{CreERT2}*ROSA*^{tdTomato} embryo. Flat-shaped endothelial cells are labeled. Scale bar, 200 μm. All error bars represent means ± SD. Statistical analysis was performed two-sided unpaired Student's *t*-test (**b** and **c**).

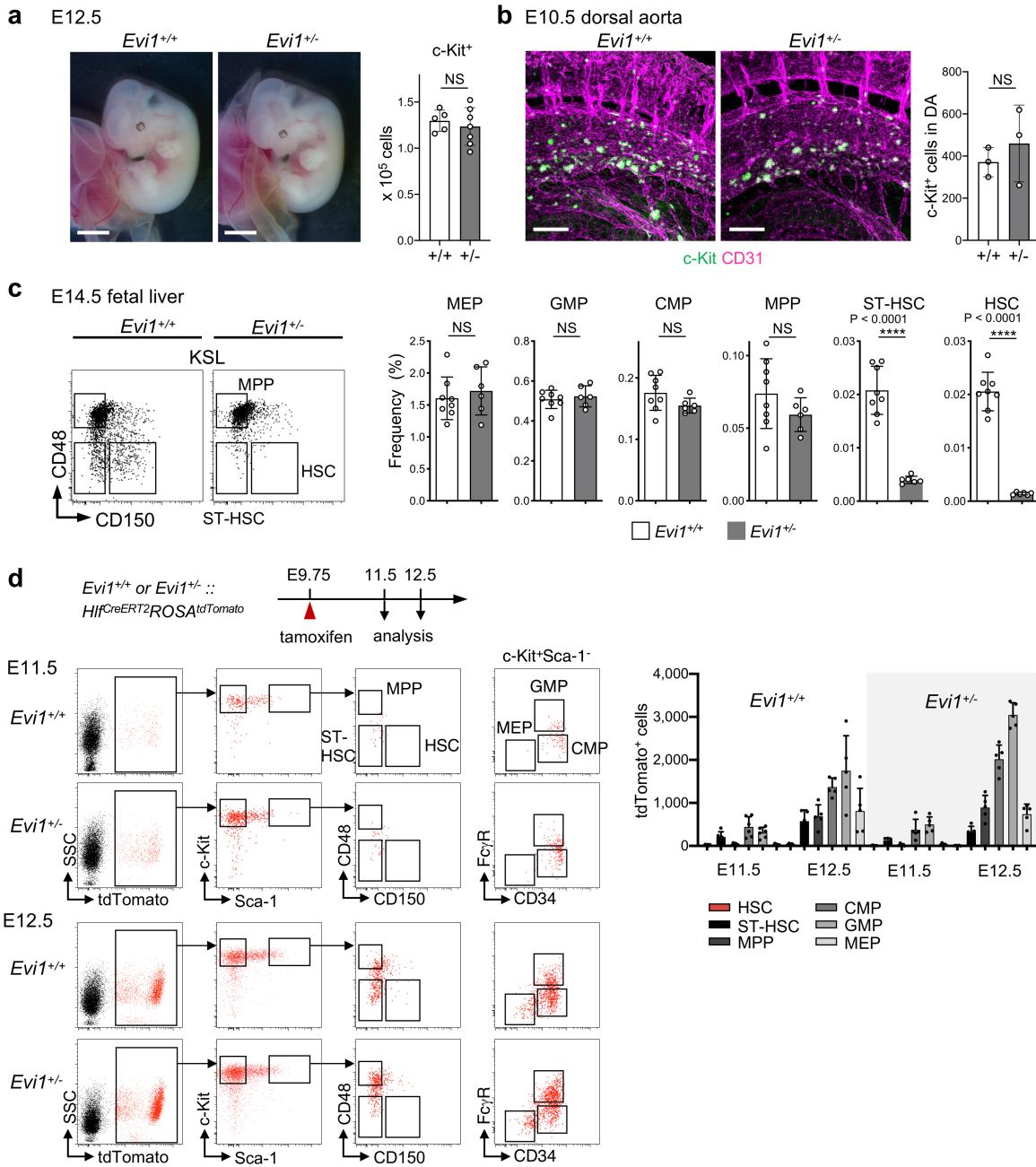


Extended Data Fig. 7 | See next page for caption.

Extended Data Fig. 7 | Evi1^{extreme hi} cells preferentially generate HSCs. **a**, Gene set enrichment analysis (GSEA) of an Evi1^{hi} subset (Hlf^{hi}c-Kit^{hi}CD45⁻ cells from caudal half region) compared with an Evi1^{lo/-} subset (Hlf^{hi}c-Kit^{hi}CD45⁻ cells from yolk sac) for HSC, MPP, and HSPC signatures. NES, normalized enrichment score; FDR, false discovery rate. **b**, Experimental design to trace the fate of Evi1^{extreme hi} cells and Evi1^{hi} cells within the same mouse (*Evi1^{CreERT2}ROSA^{tdTomato/YFP}* dual-reporter embryo). Given that the recombination rate of the *ROSA26* locus is correlated with the expression level of Evi1 (Extended Data Fig. 6d), it can be inferred that tdTomato⁺YFP⁺ cells (recombination of two *ROSA26* loci) originate from extreme Evi1 expressors. **c**, Lineage tracing of Evi1^{extreme hi} (tdTomato⁺YFP⁺) and Evi1^{hi} (tdTomato⁺YFP⁻ or tdTomato⁻YFP⁺) cells. *Evi1^{CreERT2}ROSA^{tdTomato/YFP}* embryos were administered with tamoxifen at E10.5 and were analyzed at E14.5. Top, Representative flow cytometry plots of E14.5 *Evi1^{CreERT2}ROSA^{tdTomato/YFP}* fetal liver. Bottom, Comparison of cell labeling

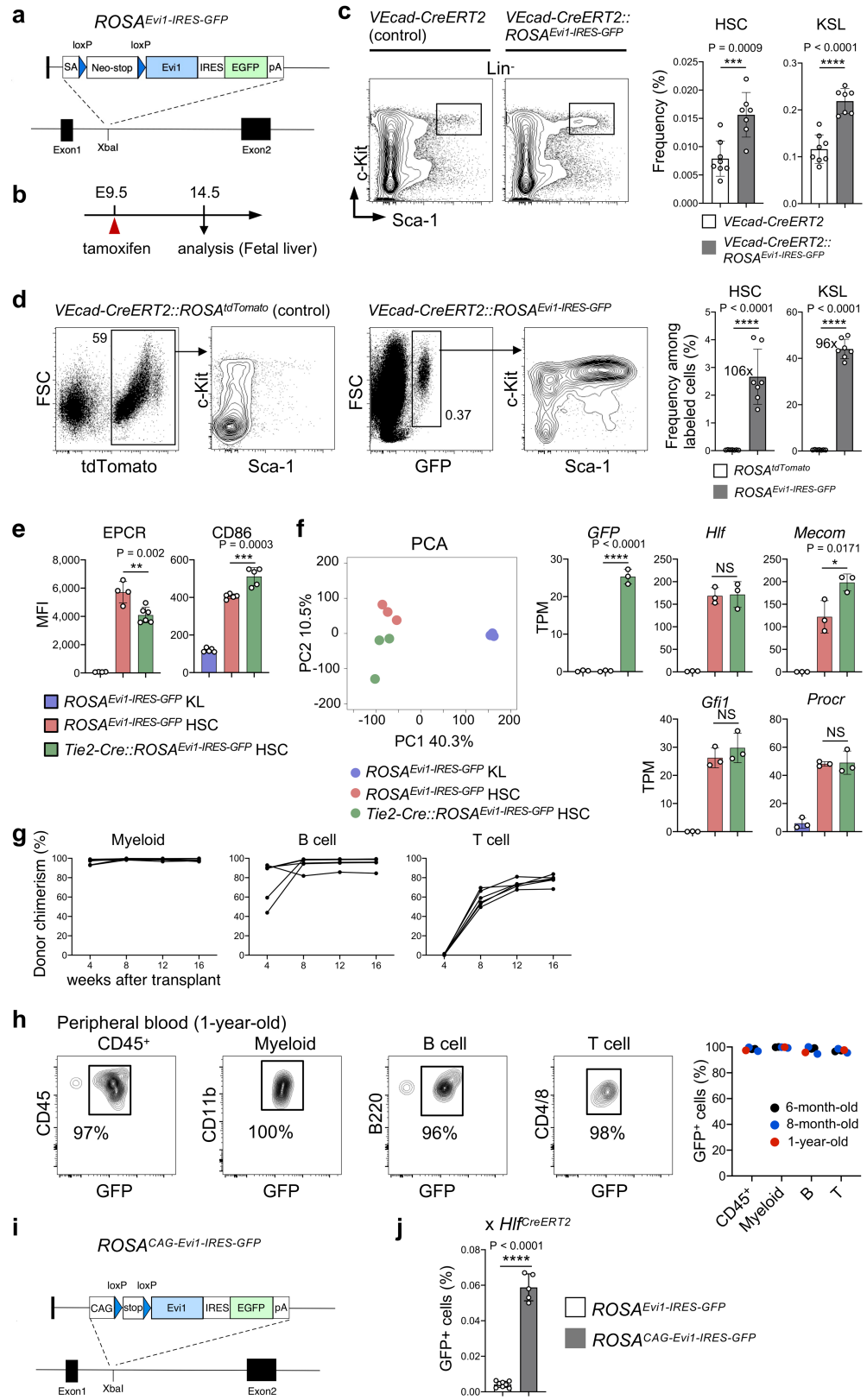
between tdTomato⁺YFP⁺ cells (Evi1^{extreme hi}-derived) and tdTomato⁺YFP⁻ or tdTomato⁻YFP⁺ cells (Evi1^{hi}-derived). n = 7. **d**, Models and expected outputs of tracing experiments. In the standard model, label frequencies of progenitors would be similar to that of HSCs. In the HSC-independent model, label frequencies of progenitors would be significantly lower than that of HSCs. **e**, Number of Hlf^{hi}c-Kit⁺ cells in E10.5 (32–36 sp) *Hlf^{tdTomato}* embryos (AGM, n = 3; yolk sac, n = 4). Number was calculated from flow cytometry data. **f**, Number of KSL (HSCs, ST-HSCs, MPPs) cells and KL (CMPs, GMPs, MEPs) cells in E14.5 fetal liver. n = 8. Number was calculated from flow cytometry data. **g**, Heterogeneity of Hlf^{hi} hematopoietic clusters in the embryo. Whole-mount immunostaining analysis of E10.5 (32 sp) *Evi1^{GFP}Hlf^{tdTomato}* embryo for tdTomato (red), GFP (green) and CD31 (white). Scale bar, 50 μm. All error bars represent means ± SD. Statistical analysis was performed two-sided unpaired Student's t-test (c).

Article



Extended Data Fig. 8 | Characterization of *Evi1*^{-/-} embryos. **a**, Analysis of E12.5 *Evi1*^{-/-} embryos. Left, Representative images of E12.5 embryos. Scale bars, 200 μ m. Right, Quantitation of c-Kit⁺ cells in the fetal liver (*Evi1*^{+/+} mice, n = 5; *Evi1*^{-/-} mice, n = 7). **b**, Normal hematopoietic cluster formation in *Evi1*^{-/-} embryos. Left, Whole-mount immunostaining of *Evi1*^{+/+} (34 sp) and *Evi1*^{-/-} (33 sp) embryos for c-Kit (green) and CD31 (magenta) expression. Scale bars, 100 μ m. Right, Number of c-Kit⁺ cells localized in the middle segment of the dorsal aorta (DA). Middle segment is 7 somite-lengths¹⁸. *Evi1*^{+/+} (n = 3, 33–35 sp); *Evi1*^{-/-} (n = 3, 33 and 34 sp). **c**, Specific decrease in stem cell fraction in *Evi1* heterozygous embryos at E14.5. Left, Representative flow cytometry plots.

Right, Frequency of HSC and progenitor fractions (*Evi1*^{+/+} mice, n = 8; *Evi1*^{-/-} mice, n = 6). Similar to the results at the E12.5 stage (Fig. 3b), severe defects were observed in the HSC fractions (15-fold decrease) in *Evi1*^{-/-} embryos at this time point. **d**, Kinetic analysis of HSC and progenitor formation from *Hif*^{CreERT2}-labeled cells in *Evi1*^{-/-} embryos. Top left, Schematic of tamoxifen treatment and analysis. Bottom left, Representative flow cytometry plots of *Hif*^{CreERT2}-labeled cells (red dots). Right, Quantitation of tdTomato⁺ cells in the fetal liver (E11.5 *Evi1*^{+/+}, n = 6; E12.5, *Evi1*^{+/+} n = 5; E11.5, *Evi1*^{-/-} n = 5; E12.5 *Evi1*^{-/-}, n = 5). All error bars represent means \pm SD. Statistical analysis was performed two-sided unpaired Student's t-test (a–c).

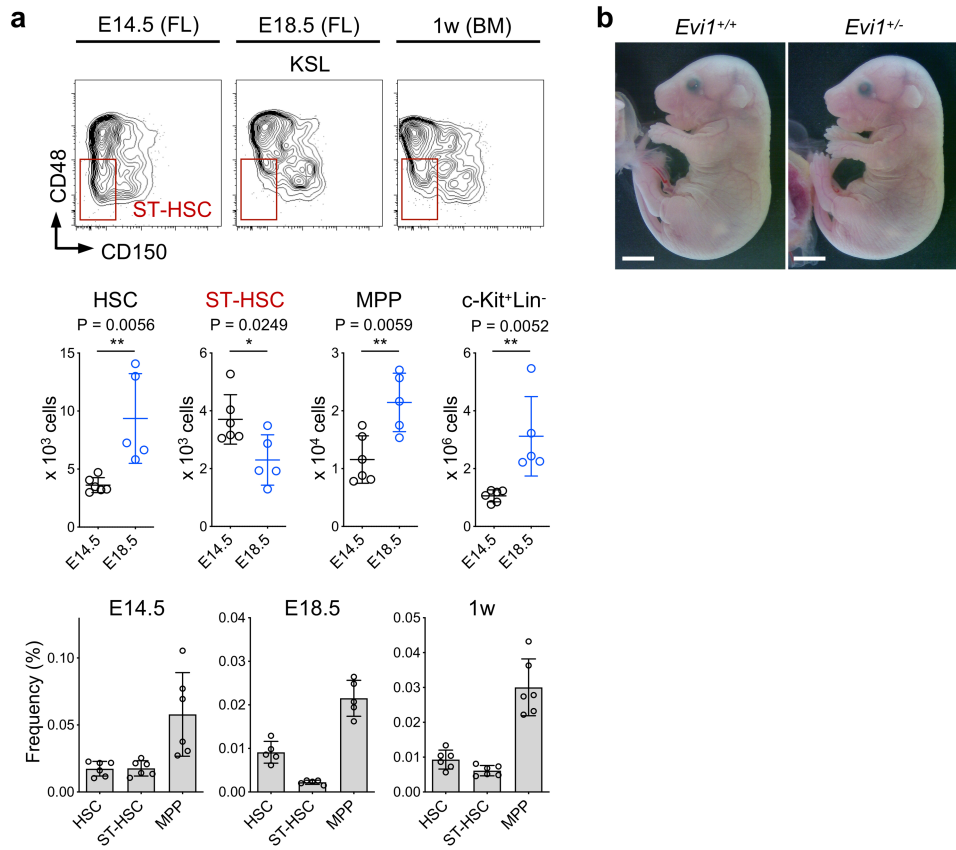


Extended Data Fig. 9 | See next page for caption.

Article

Extended Data Fig. 9 | Ectopic expression of Evil1. **a**, Targeting strategy of the *ROSA*^{*Evil1-IRES-GFP*} mouse. **b**, Schematic of tamoxifen treatment and analysis. **c**, Ectopic expression of Evil1 in VE-cadherin⁺ cells. Left, Representative flow cytometry plots. Right, Frequency of HSC and progenitor fractions (control, *VEcad-CreERT2* embryos, n = 8; *VEcad-CreERT2::ROSA*^{*Evil1-IRES-GFP*} embryos, n = 7). **d**, Fate tracing of Evil1-induced VE-cadherin⁺ cells. Left, Representative flow cytometry plots of E14.5 fetal liver cells from a *VEcad-CreERT2::ROSA*^{*tdTomato*} embryo (control) and a *VEcad-CreERT2::ROSA*^{*Evil1-IRES-GFP*} embryo. Right, Frequency of HSC and KSL in E14.5 fetal livers (*VEcad-CreERT2::ROSA*^{*tdTomato*} embryos, n = 7; *VEcad-CreERT2::ROSA*^{*Evil1-IRES-GFP*} embryos, n = 7). **e–h**, Characterization of HSCs in *Tie2-Cre::ROSA*^{*Evil1-IRES-GFP*} mice. **e**, Flow cytometry analysis of EPCR and CD86 expression. **f**, Transcriptome analysis. Left, Principal component analysis (PCA). Right, Expression of HSC-related genes, presented as transcripts per kilobase million (TPM). **g**, Transplantation experiments. Irradiated mice were

transplanted with 100 GFP⁺ HSCs isolated from E14.5 *Tie2-Cre::ROSA*^{*Evil1-IRES-GFP*} fetal liver (n = 6). Donor chimerism of myeloid, B cells, and T cells in peripheral blood was analyzed by the frequency of GFP⁺ cells. Chimerism of CD45⁺ cells is shown in Fig. 3e. **h**, Contribution of Evil1-induced cells (GFP⁺ cells) to adult hematopoiesis. Although the majority (about 70%) of *Tie2-Cre::ROSA*^{*Evil1-IRES-GFP*} mice died soon after birth for unknown reasons, the peripheral blood from the five surviving mice was analyzed (6-month-old, n = 2; 8-month old, n = 2; 1-year-old, n = 1). **i**, Targeting strategy of the *ROSA*^{*CAG-Evil1-IRES-GFP*} mouse. **j**, Frequency of GFP⁺ cells in fetal liver cells from *Hif*^{*CreERT2*}*ROSA*^{*Evil1-IRES-GFP*} (n = 8) and *Hif*^{*CreERT2*}*ROSA*^{*CAG-Evil1-IRES-GFP*} (n = 5) embryos. Embryos were administered with tamoxifen at E9.75 and were analyzed at E14.5. All error bars represent means ± SD. Statistical analysis was performed two-sided unpaired Student's t-test (**c,d** and **j**) and one-way ANOVA with Tukey-Kramer test (**e** and **f**).



Extended Data Fig. 10 | Decrease in ST-HSC at late gestation. **a**, Analysis of the KSL fraction. Top, Representative flow cytometry plots of the KSL fraction in E14.5 fetal livers (FL), E18.5 FL and 1-week bone marrow (BM). Middle, Comparison of HSPC fractions between E14.5 and E18.5. Number of HSCs, ST-HSCs, MPP, and c-Kit⁺Lin⁻ cells. HSPC, hematopoietic stem and progenitor

cells; KSL, c-Kit⁺Sca-1⁺Lineage⁻. Bottom, Frequency of HSC and progenitors (E14.5 embryos, n = 6; E18.5 embryos, n = 5; 1w mice, n = 6). **b**, Representative images of E18.5 embryos. Scale bars, 300 μ m. All error bars represent means \pm SD. Statistical analysis was performed two-sided unpaired Student's t-test (a).

Reporting Summary

Nature Research wishes to improve the reproducibility of the work that we publish. This form provides structure for consistency and transparency in reporting. For further information on Nature Research policies, see our [Editorial Policies](#) and the [Editorial Policy Checklist](#).

Statistics

For all statistical analyses, confirm that the following items are present in the figure legend, table legend, main text, or Methods section.

n/a Confirmed

- The exact sample size (n) for each experimental group/condition, given as a discrete number and unit of measurement
- A statement on whether measurements were taken from distinct samples or whether the same sample was measured repeatedly
- The statistical test(s) used AND whether they are one- or two-sided
Only common tests should be described solely by name; describe more complex techniques in the Methods section.
- A description of all covariates tested
- A description of any assumptions or corrections, such as tests of normality and adjustment for multiple comparisons
- A full description of the statistical parameters including central tendency (e.g. means) or other basic estimates (e.g. regression coefficient) AND variation (e.g. standard deviation) or associated estimates of uncertainty (e.g. confidence intervals)
- For null hypothesis testing, the test statistic (e.g. F , t , r) with confidence intervals, effect sizes, degrees of freedom and P value noted
Give P values as exact values whenever suitable.
- For Bayesian analysis, information on the choice of priors and Markov chain Monte Carlo settings
- For hierarchical and complex designs, identification of the appropriate level for tests and full reporting of outcomes
- Estimates of effect sizes (e.g. Cohen's d , Pearson's r), indicating how they were calculated

Our web collection on [statistics for biologists](#) contains articles on many of the points above.

Software and code

Policy information about [availability of computer code](#)

Data collection

Microscopes
Olympus FV-1200; FV10-ASW v04.02
Nikon A1 HD25; NIS-Elements AR 5.21

Flow cytometry
BD FACS AriaIII; FACSDiva v8.0.1
BD FACS Cantor; FACSDiva v8.0.1
BD FACSymphony; FACSDiva v9.1

RNA-seq
Illumina HiSeqX platform (single-cell)
Illumina NextSeq platform (bulk)

Data analysis

Image analysis; Fiji (1.53a), Imaris (v8.2.0; Bitplane), Olympus FV10-ASW (v04.02)
Flow cytometry; FlowJo (v9.9.6 and v10.7.1)
Statistical analysis; GraphPad Prism (v8.4.3)
RNA-seq analysis; R (v3.6.1), Cell Ranger (v5.0.0; 10x Genomics), Surat (v4.0.0), uwot (v0.1.10), Loupe Browser software (10x Genomics), HISAT2 (v2.1.0), StringTie (v2.1.2), edgeR (v3.26.8), GSEA (v4.1.0)

For manuscripts utilizing custom algorithms or software that are central to the research but not yet described in published literature, software must be made available to editors and reviewers. We strongly encourage code deposition in a community repository (e.g. GitHub). See the Nature Research [guidelines for submitting code & software](#) for further information.

Data

Policy information about [availability of data](#)

All manuscripts must include a [data availability statement](#). This statement should provide the following information, where applicable:

- Accession codes, unique identifiers, or web links for publicly available datasets
- A list of figures that have associated raw data
- A description of any restrictions on data availability

The bulk and single-cell RNA-seq datasets have been deposited at the Gene Expression Omnibus (GEO) repository with the following accession numbers: GSE168054 (bulk), GSE190011 (bulk), and GSE167932 (single-cell).

scRNA-seq data (GSE143637 and GSE150412) are available at GEO.

Source data are provided with this paper.

Field-specific reporting

Please select the one below that is the best fit for your research. If you are not sure, read the appropriate sections before making your selection.

Life sciences Behavioural & social sciences Ecological, evolutionary & environmental sciences

For a reference copy of the document with all sections, see nature.com/documents/nr-reporting-summary-flat.pdf

Life sciences study design

All studies must disclose on these points even when the disclosure is negative.

Sample size	Sample size was not predetermined because it is difficult to predict in advance the number of embryos of a particular genotype in each litter. However, the number of timed matings was adjusted so that the number of embryos to be analyzed was as small as possible while still allowing for sufficient statistical analysis.
Data exclusions	Fig.1g top right graph; one fetal liver sample (E10.5) was removed because severe damage was observed after immunostaining.
Replication	Experimental data obtained from FACS analysis was replicated using at least 3 independent biological samples. Representative micrographs came from at least two biological replicates (summarized in Supplementary Table 2).
Randomization	Samples and animals were assigned to groups randomly. Male and female embryos were used for the study.
Blinding	Blinding was not performed to efficiently analyze specific genotypes and reduce the number of mice analyzed. However, all experiments were performed in the same workflow.

Reporting for specific materials, systems and methods

We require information from authors about some types of materials, experimental systems and methods used in many studies. Here, indicate whether each material, system or method listed is relevant to your study. If you are not sure if a list item applies to your research, read the appropriate section before selecting a response.

Materials & experimental systems

n/a	Involved in the study
<input type="checkbox"/>	<input checked="" type="checkbox"/> Antibodies
<input checked="" type="checkbox"/>	<input type="checkbox"/> Eukaryotic cell lines
<input checked="" type="checkbox"/>	<input type="checkbox"/> Palaeontology and archaeology
<input type="checkbox"/>	<input checked="" type="checkbox"/> Animals and other organisms
<input checked="" type="checkbox"/>	<input type="checkbox"/> Human research participants
<input checked="" type="checkbox"/>	<input type="checkbox"/> Clinical data
<input checked="" type="checkbox"/>	<input type="checkbox"/> Dual use research of concern

Methods

n/a	Involved in the study
<input checked="" type="checkbox"/>	<input type="checkbox"/> ChIP-seq
<input type="checkbox"/>	<input checked="" type="checkbox"/> Flow cytometry
<input checked="" type="checkbox"/>	<input type="checkbox"/> MRI-based neuroimaging

Antibodies

Antibodies used

CD3e-PerCP-Cy5.5, clone 145-2C11, 1:50, BioLegend, cat# 100328, Flow cytometry
 CD4-PerCP-Cy5.5, clone RM4-5, 1:100, BioLegend, cat# 100540, Flow cytometry
 CD4-APC, clone RM4-5, 1:100, BioLegend, cat# 100516, Flow cytometry
 CD4-APC-Cy7, clone RM4-5, 1:100, BioLegend, cat# 100526, Flow cytometry
 CD8a-PerCP-Cy5.5, clone 53-6.7, 1:100, BioLegend, cat# 100734, Flow cytometry
 CD8a-APC, clone 53-6.7, 1:100, BioLegend, cat# 100712, Flow cytometry
 CD8a-APC-Cy7, clone 53-6.7, 1:100, BioLegend, cat# 100714, Flow cytometry

CD16/32-APC, clone 93, 1:100, BioLegend, cat# 101326, Flow cytometry
 CD16/32-APC-Cy7, clone 93, 1:100, BioLegend, cat# 101328, Flow cytometry
 CD31, clone 2H8, 1:1000, Merck, cat# MAB1398Z, Immunofluorescence
 CD31-Biotin, clone MEC13.3, 1:500, BD Biosciences, cat# 553371, Immunofluorescence
 CD31-FITC, clone MEC13.3, 1:100, BD Biosciences, cat# 553372, Flow cytometry
 CD31-BV421, clone MEC13.3, 1:100, BD Biosciences, cat# 562939, Flow cytometry
 CD34-FITC, clone RAM34, 1:50, eBioscience, cat# 11-0341-85, Flow cytometry
 CD34-Alexa Fluor 647, clone RAM34, 1:25, BD Biosciences, cat# 560230, Flow cytometry
 CD41-PerCP-eFluor 710, clone MWReg30, 1:100, eBioscience, cat# 46-0411-82, Flow cytometry
 CD41-APC-Cy7, clone MWReg30, 1:100, BioLegend, cat# 133928, Flow cytometry
 CD45-APC-Cy7, clone 30-F11, 1:200, BD Biosciences, cat# 557659, Flow cytometry
 CD45-BV510, clone 30-F11, 1:100, BD Biosciences, cat# 563891, Flow cytometry
 CD45.1-FITC, clone A20, 1:400, BioLegend, cat# 110706, Flow cytometry
 CD45.2-APC, clone 104, 1:200, BioLegend, cat# 109814, Flow cytometry
 CD48-FITC, clone HM48-1, 1:50, BioLegend, cat# 103404, Flow cytometry
 CD48-PE, clone HM48-1, 1:200, BioLegend, cat# 103406, Flow cytometry
 CD86-APC, clone GL1, 1:50, BD Biosciences, cat# 558703, Flow cytometry
 CD150-BV421, clone TC15-12F12.2, 1:50, BioLegend, cat# 115926, Flow cytometry
 B220-PerCP-Cy5.5, clone RA3-6B2, 1:50, BioLegend, cat# 103236, Flow cytometry
 B220-PE-Cy7, clone RA3-6B2, 1:200, BioLegend, cat# 103222, Flow cytometry
 c-Kit, goat, 1:2000, RnD Systems, cat# AF1356, Immunofluorescence
 c-Kit, clone 2B8, 1:500, BD Biosciences, cat# 553352, Immunofluorescence
 c-Kit-PE-Cy7, clone 2B8, 1:400, BioLegend, cat# 105814, Flow cytometry
 c-Kit-APC, clone 2B8, 1:200, BioLegend, cat# 105812, Flow cytometry
 c-Kit-BV421, clone 2B8, 1:200, BioLegend, cat# 105828, Flow cytometry
 EPCR-APC, clone eBio1560, 1:150, eBioscience, cat# 17-2012-82, Flow cytometry
 Flt3-APC, clone A2F10, 1:100, BioLegend, cat# 135310, Flow cytometry
 Gr-1-PE, clone RB6-8C5, 1:200, BioLegend, cat# 108408, Flow cytometry
 Gr-1-PerCP-Cy5.5, clone RB6-8C5, 1:200, BioLegend, cat# 108428, Flow cytometry
 IL-7Ra-BV421, clone A7R34, 1:20, BioLegend, cat# 135024, Flow cytometry
 Mac-1-FITC, clone M1/70, 1:100, BD Biosciences, cat# 553310, Flow cytometry
 Mac-1-PE, clone M1/70, 1:200, BioLegend, cat# 101208, Flow cytometry
 Mac-1-PerCP-Cy5.5, clone M1/70, 1:100, BioLegend, cat# 101228, Flow cytometry
 Sca-1-PE-Cy7, clone D7, 1:400, BioLegend, cat# 108114, Flow cytometry
 Ter119-FITC, clone TER-119, 1:200, BioLegend, cat# 116206, Flow cytometry
 Ter119-PerCP-Cy5.5, clone TER-119, 1:100, BioLegend, cat# 116228, Flow cytometry
 GFP, rabbit, 1:2000, MBL, cat# 598, Immunofluorescence
 RFP, rabbit, 1:1000, Rockland, cat# 600-401-379, Immunofluorescence
 Alexa Fluor 488 AffiniPure goat anti-armenian hamster IgG (H+L), 1:5000, Jackson ImmunoResearch, cat# 127-545-160, Immunofluorescence
 Alexa Fluor 488 donkey anti-goat IgG (H+L), 1:5000, Invitrogen, cat# A32814, Immunofluorescence
 Cy3 AffiniPure F(ab')2 Fragment donkey anti-rat IgG (H+L), 1:5000, Jackson ImmunoResearch, cat# 712-166-153, Immunofluorescence
 Cy3 AffiniPure F(ab')2 Fragment donkey anti-rabbit IgG (H+L), 1:5000, Jackson ImmunoResearch, cat# 711-166-152, Immunofluorescence
 Alexa Fluor 647 donkey anti-rat IgG (H+L), 1:5000, Invitrogen, cat# A48272, Immunofluorescence
 Alexa Fluor 647 goat anti-rabbit IgG (H+L), 1:5000, Invitrogen, cat# A21244, Immunofluorescence
 Alexa Fluor 647 AffiniPure goat anti-armenian hamster IgG (H+L), 1:5000, Jackson ImmunoResearch, cat# 127-605-160, Immunofluorescence

Validation

All antibodies are commercially available and were validated based on information provided by the supplier. Titration experiments were performed prior to the study.

CD3e, BioLegend, <https://www.biologend.com/en-us/products/percp-cyanine5-5-anti-mouse-cd3epsilon-antibody-4191>
 CD4, BioLegend, <https://www.biologend.com/en-us/products/percp-cyanine5-5-anti-mouse-cd4-antibody-4230>
 CD8a, BioLegend, <https://www.biologend.com/en-us/products/percp-cyanine5-5-anti-mouse-cd8a-antibody-4255>
 CD16/32, BioLegend, <https://www.biologend.com/en-us/products/apc-anti-mouse-cd16-32-antibody-6282>
 CD31, Merck, https://www.emdmillipore.com/US/en/product/Anti-PECAM-1-Antibody-clone-2H8-Azide-Free,MM_NF-MAB1398Z?bd=1
 CD31, BD Biosciences, <https://www.bdbiosciences.com/us/applications/research/stem-cell-research/cancer-research/mouse/biotin-rat-anti-mouse-cd31-mec-133/p/553371>
 CD34, eBioscience, <https://www.thermofisher.com/antibody/product/CD34-Antibody-clone-RAM34-Monoclonal/11-0341-82?imageId=89577>
 CD34, BD Biosciences, <https://www.bdbiosciences.com/us/applications/research/stem-cell-research/cancer-research/mouse/alex-fluor-647-rat-anti-mouse-cd34-ram34/p/560233>
 CD41, eBioscience, <https://www.thermofisher.com/antibody/product/CD41a-Antibody-clone-eBioMWReg30-MWReg30-Monoclonal/46-0411-82>
 CD41, BioLegend, <https://www.biologend.com/en-us/products/apc-cyanine7-anti-mouse-cd41-antibody-1304>
 CD45, BD Biosciences, <https://www.bdbiosciences.com/us/applications/research/stem-cell-research/cancer-research/mouse/apc-cy7-rat-anti-mouse-cd45-30-f11/p/557659>
 CD45.1, BioLegend, <https://www.biologend.com/en-us/search-results/fitc-anti-mouse-cd45-1-antibody-198>
 CD45.2, BioLegend, <https://www.biologend.com/en-us/search-results/apc-anti-mouse-cd45-2-antibody-2759>
 CD48, BioLegend, <https://www.biologend.com/en-us/products/fitc-anti-mouse-cd48-antibody-291>
 CD86, BD Biosciences, <https://www.bdbiosciences.com/ja-jp/products/reagents/flow-cytometry-reagents/research-reagents/single-color-antibodies-ruo/apc-rat-anti-mouse-cd86.561964>
 CD150, BioLegend, <https://www.biologend.com/en-us/products/brilliant-violet-421-anti-mouse-cd150-slam-antibody-7162>

B220, BioLegend, <https://www.biologegend.com/en-us/products/percp-cyanine5-5-anti-mouse-human-cd45r-b220-antibody-4267>
 c-Kit, RnD Systems, https://www.rndsystems.com/products/human-mouse-cd117-c-kit-antibody_af1356
 c-Kit, BD Biosciences, <https://www.bdbsciences.com/us/applications/research/stem-cell-research/cancer-research/mouse/purified-rat-anti-mouse-cd117-2b8/p/553352>
 c-Kit, BioLegend, <https://www.biologegend.com/en-us/products/pe-cyanine7-anti-mouse-cd117-c-kit-antibody-1900>
 EPCR, eBioscience, <https://www.thermofisher.com/antibody/product/CD201-EPCR-Antibody-clone-eBio1560-1560-Monoclonal/17-2012-82?imageId=709426>
 Flt3, BioLegend, <https://www.biologegend.com/en-us/search-results/apc-anti-mouse-cd135-antibody-6284>
 Gr-1, BioLegend, <https://www.biologegend.com/en-us/products/percp-cyanine5-5-anti-mouse-ly-6g-ly-6c-gr-1-antibody-4286>
 IL-7Ra, BioLegend, <https://www.biologegend.com/en-us/search-results/brilliant-violet-421-anti-mouse-cd127-il-7ralpha-antibody-7193>
 Mac-1, BD Biosciences, <https://www.bdbsciences.com/us/applications/research/stem-cell-research/mesenchymal-stem-cell-markers-bone-marrow/mouse/negative-markers/fitc-rat-anti-cd11b-m170/p/553310>
 Mac-1, BioLegend, <https://www.biologegend.com/en-us/products/percp-cyanine5-5-anti-mouse-human-cd11b-antibody-4257>
 Sca-1, BioLegend, <https://www.biologegend.com/en-us/products/pe-cyanine7-anti-mouse-ly-6a-e-sca-1-antibody-3137>
 Ter119, BioLegend, <https://www.biologegend.com/en-us/products/fitc-anti-mouse-ter-119-erythroid-cells-antibody-1865>
 GFP, MBL, <https://ruo.mbl.co.jp/bio/e/dtl/A/?pcd=598>
 RFP, Rockland, https://rockland-inc.com/store/Antibodies-to-GFP-and-Antibodies-to-RFP-600-401-379-O4L_24299.aspx
 Alexa Fluor 488 AffiniPure goat anti-armenian hamster IgG (H+L), Jackson ImmunoResearch, <https://www.jacksonimmuno.com/catalog/products/127-545-160>
 Alexa Fluor 488 donkey anti-goat IgG (H+L), Invitrogen, <https://www.thermofisher.com/antibody/product/Donkey-anti-Goat-IgG-H-L-Highly-Cross-Adsorbed-Secondary-Antibody-Polyclonal/A32814>
 Cy3 AffiniPure F(ab')2 Fragment donkey anti-rat IgG (H+L), Jackson ImmunoResearch, <https://www.jacksonimmuno.com/catalog/products/712-166-153>
 Cy3 AffiniPure F(ab')2 Fragment donkey anti-rabbit IgG (H+L), Jackson ImmunoResearch, <https://www.jacksonimmuno.com/catalog/products/711-166-152>
 Alexa Fluor 647 donkey anti-rat IgG (H+L), Invitrogen, <https://www.thermofisher.com/antibody/product/Donkey-anti-Rat-IgG-H-L-Highly-Cross-Adsorbed-Secondary-Antibody-Polyclonal/A48272>
 Alexa Fluor 647 goat anti-rabbit IgG (H+L), Invitrogen, <https://www.thermofisher.com/antibody/product/Goat-anti-Rabbit-IgG-H-L-Cross-Adsorbed-Secondary-Antibody-Polyclonal/A-21244>
 Alexa Fluor 647 AffiniPure goat anti-armenian hamster IgG (H+L), Jackson ImmunoResearch, <https://www.jacksonimmuno.com/catalog/products/127-605-160>

Animals and other organisms

Policy information about [studies involving animals; ARRIVE guidelines](#) recommended for reporting animal research

Laboratory animals

Mus musculus was used as an animal model. All mice used in this study were C57BL/6 background, except for foster mothers (ICR). Males and females were used for the study. Embryos were analyzed from E9.5 to 18.5 (E9.5, E10.5, E11.25, E11.5, E12.5, E13.5, E14.5 and E18.5) and adult mice were collected at 1w-8mo (1w, 2w, 4w, 8w, 11w and 8mo). The strains used in this study are shown as below.

1. Hlf-tdTomato (Yokomizo et al., 2019)
2. Runx1-CreERT2 (Matsuo et al., 2017, CARD2327)
3. VEcad-CreERT2 (Okabe et al., 2014)
4. ROSA-tdTomato (Madisen et al., 2010, JAX007914)
5. ROSA-YFP (Srinivas et al., 2001, JAX006148)
6. Vav-iCre (de Boer et al., 2003, JAX008610)
7. Tie2-Cre (Kisanuki et al., 2001, JAX008863)
8. Evi1+- (Goyama et al., 2008)
9. Evi1-GFP (Kataoka et al., 2011)
10. Hlf-CreERT2 (this paper)
11. Evi1-CreERT2 (this paper)
12. ROSA-Evi1-IRES-GFP (this paper)
13. ROSA-CAG-Evi1-IRES-GFP (this paper)
14. C57BL/6J (Japan SLC)
15. C57BL/6N (Japan SLC)
16. ICR (Japan SLC)
17. C57BL/6-Ly5.1 (Sankyo-Lab Service)

All mice were bred in a specific pathogen-free animal facility (12 h light and 12 h darkness) at Kumamoto University.

Wild animals

The study did not use any wild animals

Field-collected samples

The study did not include field-collected samples

Ethics oversight

All animal experiments were performed in accordance with institutional guidelines and were approved by the Animal Care and Use Committee of Kumamoto University (Approved No. A20-092 and A2019-093).

Note that full information on the approval of the study protocol must also be provided in the manuscript.

Flow Cytometry

Plots

Confirm that:

- The axis labels state the marker and fluorochrome used (e.g. CD4-FITC).
- The axis scales are clearly visible. Include numbers along axes only for bottom left plot of group (a 'group' is an analysis of identical markers).
- All plots are contour plots with outliers or pseudocolor plots.
- A numerical value for number of cells or percentage (with statistics) is provided.

Methodology

Sample preparation

AGM, yolk sac and placenta: Single-cell suspensions were prepared by treating tissues with collagenase [0.125% in PBS/10% fetal calf serum (FCS)/1% penicillin/streptomycin] for 1 h at 37°C.
Fetal liver was dissected and minced with 21G syringe needle.
Bone marrow cells were prepared by crushing the bones using a mortar.

Instrument

BD FACS AriaIII, FACS Canto II, and FACSymphony

Software

BD FACSDiva (v8.0.1 and v9.1) and FlowJo (v9.9.6 and v10.7.1)

Cell population abundance

Purity check was performed on a small fraction of sorted cells (>95%).

Gating strategy

Combinations of cell-surface markers and transcription factor (Hlf-tdTomato reporter) were used to identify the following populations: HSC (CD150+CD48-c-Kit+Sca-1+Lineage-), ST-HSC (CD150-CD48-c-Kit+Sca-1+Lineage-), MPP (CD150-CD48+c-Kit +Sca-1+Lineage-), CMP (CD34+FcgR-c-Kit+Sca-1-Lineage-), GMP (CD34+FcgR+c-Kit+Sca-1-Lineage-), MEP (CD34-FcgR-c-Kit +Sca-1-Lineage-), EMP (c-Kit+CD41+CD16/32+), LMP (c-Kit+CD45+IL7Ra+Flt3+Lineage-), Hematopoietic cluster cells (Hlf+c-Kit +), Endothelial cells (CD31+CD45-CD41-), Erythrocytes (Ter119+CD41-), Platelets (CD41+Ter119-), Myeloid cells (CD11b+Gr-1+), B cell (B220+CD4-CD8-CD11b-), T cell (CD4/8+B220-CD11b-).
Doublets were excluded by forward scatter width/height (FSC-W/FSC-H) and side scatter width/height (SSC-W/SSC-H) gating.
Dead cells were excluded by Hoechst33258 or PI staining.

- Tick this box to confirm that a figure exemplifying the gating strategy is provided in the Supplementary Information.